ACS NANOSCIENCE Au
AN OPEN ACCESS JOURNAL OF THE AMERICAN CHEMICAL SOCIETY

pubs.acs.org/nanoau
Review

Two-Dimensional Electrically Conductive Metal–Organic Frameworks as Chemiresistive Sensors

Chungseong Park, Jong Won Baek, Euichul Shin, and Il-Doo Kim*

Cite This: ACS Nanosci. Au 2023, 3, 353–374
Read Online

ACCESS | Metrics & More | Article Recommendations

ABSTRACT: Metal–organic frameworks (MOFs) have emerged as attractive chemical sensing materials due to their exceptionally high porosity and chemical diversity. Nevertheless, the utilization of MOFs in chemiresistive type sensors has been hindered by their inherent limitation in electrical conductivity. The recent emergence of two-dimensional conductive MOFs (2D c-MOFs) has addressed this limitation by offering enhanced electrical conductivity, while still retaining the advantageous properties of MOFs. In particular, c-MOFs have shown promising advantages for the fabrication of sensors capable of operating at room temperature. Thus, active research on gas sensors utilizing c-MOFs is currently underway, focusing on enhancing sensitivity and selectivity. To comprehend the potential of MOFs as chemiresistive sensors for future applications, it is crucial to understand not only the fundamental properties of conductive MOFs but also the state-of-the-art works that contribute to improving their performance. This comprehensive review delves into the distinctive characteristics of 2D c-MOFs as a new class of chemiresistors, providing in-depth insights into their unique sensing properties. Furthermore, we discuss the proposed sensing mechanisms associated with 2D c-MOFs and provide a concise summary of the strategies employed to enhance the sensing performance of 2D c-MOFs. These strategies encompass a range of approaches, including the design of metal nodes and linkers, morphology control, and the synergistic use of composite materials. In addition, the review thoroughly explores the prospects of 2D c-MOFs as chemiresistors and elucidates their remarkable potential for further advancements. The insights presented in this review shed light on future directions and offer valuable opportunities in the chemical sensing research field.

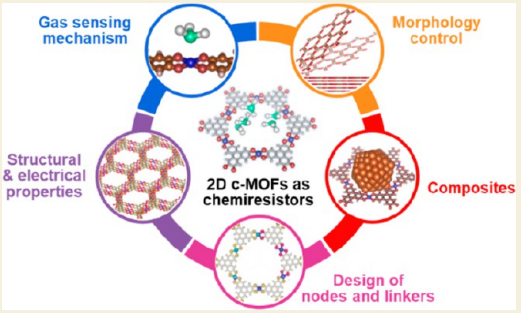

KEYWORDS: *metal–organic frameworks, chemiresistors, two-dimensional materials, sensors, electrical conductivity, sensing mechanism, selectivity, sensitivity, composites*

1. INTRODUCTION

Metal–organic frameworks (MOFs) are a unique class of porous materials constructed from metal nodes and organic linkers. Due to their inherent permanent porosity and chemical tunability, MOFs have found widespread applications in diverse fields, including gas storage,[1−3] catalysis,[4−6] energy storage,[7−9] and separation processes.[10−12] Among these applications, chemical sensing emerges as an ideal and prominent research field for the utilization of MOFs.[13,14] The remarkable porosity of MOFs facilitates the easy diffusion of analytes, while the tunability of these materials enables the incorporation of various binding sites, leading to specific interaction with target gases.[15] These unique properties make MOFs highly suitable for chemical sensing applications. Among various types of sensors, chemiresistive sensors simultaneously offer high cost-effectiveness, portability, and sensitivity.[16,17] However, conventional MOFs, lacking efficient charge transport pathways through their abundant pores, have been considered as electrically insulating materials, limiting their use in chemiresistors. Despite efforts to utilize MOFs with narrow band gaps in chemiresistors, their limited conductivities still require thermal activation, which poses challenges in terms of stability and device complexity.[18−20] Alternatively, MOFs can be employed in conjunction with other conductive materials. However, in such cases, the interaction of MOFs may not be entirely transduced into the electrical signal, resulting in poor responses.[21]

However, the recent emergence of two-dimensional conductive MOFs (2D c-MOFs) has opened up new possibilities for the application of MOFs in various electronic devices as active components.[22−26] 2D c-MOFs are composed of π-conjugated ligands capable of effective charge delocalization. These ligands are linked to metal nodes through π–d

Received: June 10, 2023
Revised: July 24, 2023
Accepted: July 24, 2023
Published: August 9, 2023

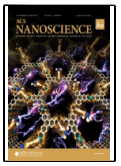

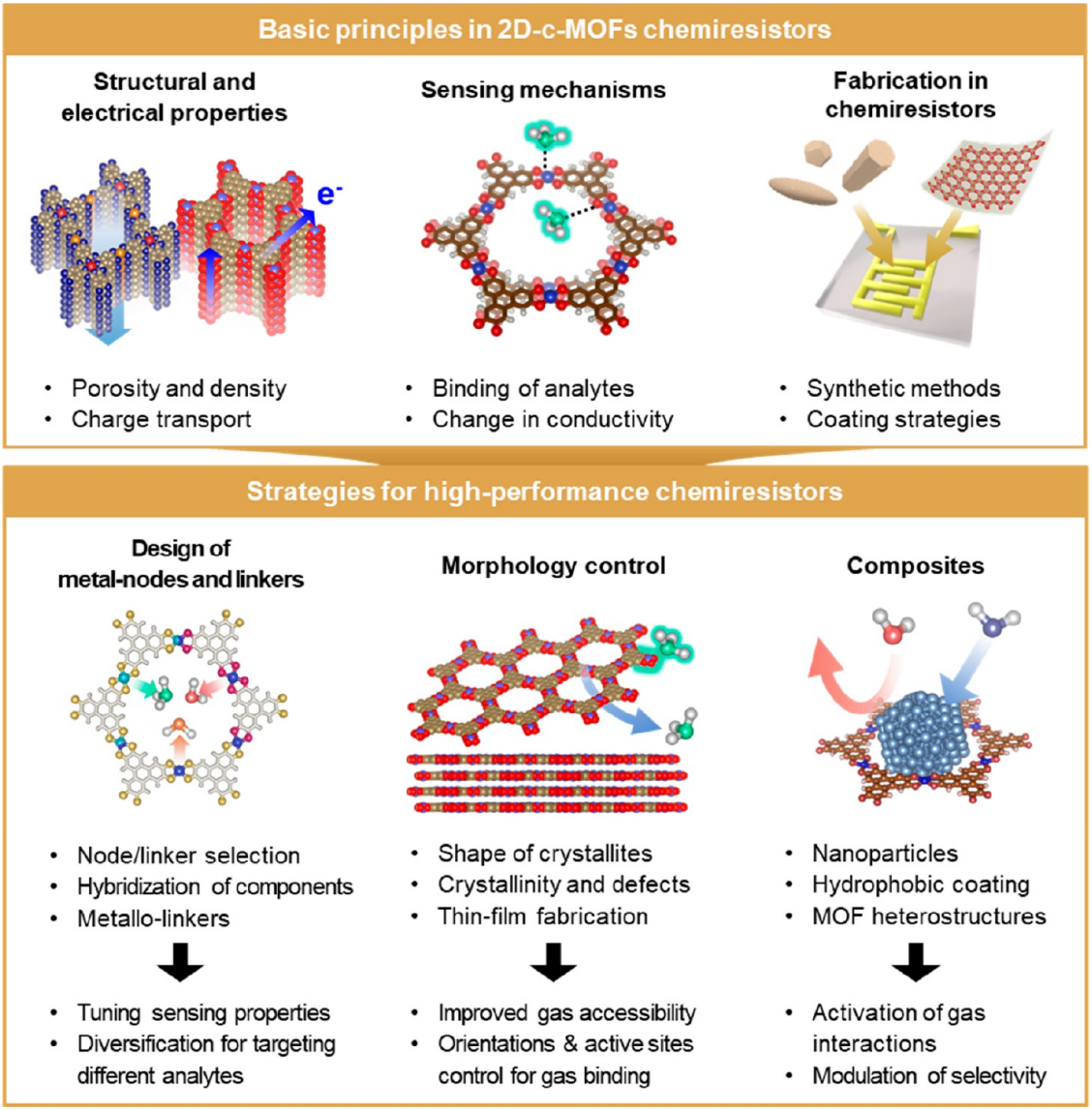

Figure 1. Overview of basic principles of 2D c-MOFs in the context of chemiresistors, and strategies for improving the sensing performance with their key advantages.

hybridization, forming extended conjugation throughout the frameworks. As a result, 2D c-MOFs offer sufficiently high electrical conductivity measurable at room temperature, combined with the advantageous properties of MOFs. In 2D c-MOFs, the facile gas adsorption and interactions via various active sites can be directly transduced into an electrical signal, making them highly desirable materials for chemiresistive sensors.

Due to the unique properties described above, 2D c-MOFs exhibit several advantages over other sensing materials, such as metal oxides,[27−29] graphene,[30−33] and transition metal dichalcogenide.[34−36] First, 2D c-MOFs inherently offer tunable porous structures, which are a key design element in sensing materials. Unlike other sensing materials that require multiple nanostructuring processes to achieve efficient porous structures,[37−39] as-synthesized 2D c-MOFs provide well-defined porous structures with higher porosity and surface area. This feature simplifies the fabrication process of sensors, allowing for improved gas adsorption and interactions within the material, thereby enhancing sensing performance. Second, 2D c-MOFs possess highly tunable electrical properties. The high electrical conductivity and room temperature operation of 2D c-MOFs offer a significant advantage by addressing the issues associated with thermally activated sensors, which typically operate at elevated temperatures ranging from 200 to 400 °C. By eliminating the need for such high-temperature operation, 2D c-MOFs can overcome challenges related to device complexity, power consumption, and instability.[40−42] Furthermore, the conductivity of 2D c-MOFs can be easily tuned across a wide range, enabling the utilization of sensors with optimal intrinsic conductivity depending on specific measurement conditions.[43,44] This makes 2D c-MOFs more practical and efficient for room temperature chemiresistive sensing application. Third, the high diversity in chemical structures of 2D c-MOFs provides an advantage in selectivity tuning. Semiconducting metal oxides, which are the most well-established chemiresistive sensing materials, have achieved a sufficiently high level of sensitivity.[45−48] However, the selective detection of target gases in real environments, where interfering gases are present, continues to be a significant

https://doi.org/10.1021/acsnanoscienceau.3c00024
ACS Nanosci. Au 2023, 3, 353−374

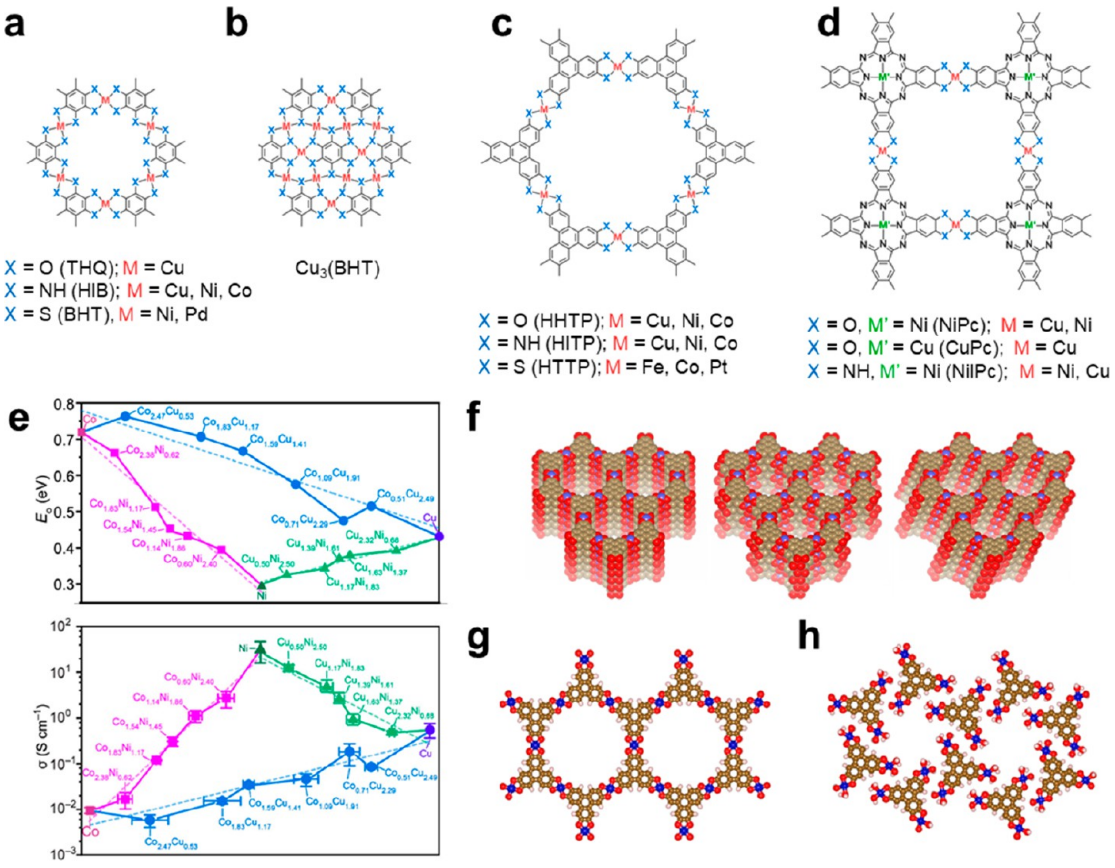

Figure 2. Structure of lattice layers in (a) benzene-based 2D c-MOFs, (b) Cu_3(BHT), (c) triphenylene-based 2D c-MOFs, and (d) phthalocyanine-based 2D c-MOFs. (e) Variation in bandgaps and conductivities of $M_3(HITP)_2$ with Co, Cu, and Ni nodes. Reprinted with permission from ref 88. Copyright 2020 American Chemical Society. (f) Possible stacking arrangements (eclipsed, serrated, and inclined) of 2D layers. Structures of (g) extended frameworks and (h) discrete complexes.

challenge.[17] This is because metal oxides primarily rely on similar surface reactions involving chemisorbed oxygen when interacting with different analytes.[49] In contrast, the high diversity of binding sites in 2D c-MOFs enables unique interactions for specific targets, offering great potential to address these challenges associated with selective detection in the presence of interfering gases. In recent years, significant progress has been made in the development of 2D c-MOF-based sensors, demonstrating their potential as promising sensing materials. However, a dedicated review paper specifically focusing on the application of 2D c-MOFs in chemiresistors is currently lacking, while there are review papers discussing the applications of MOFs in sensors[50−55] or 2D c-MOFs-based electronics in a more general context.[22,56,57]

In this review, our objective is to provide comprehensive insights into the application of 2D c-MOFs as chemiresistors, offering cutting-edge sensing strategies and a deeper understanding of their unique characteristics relevant to sensing performance (Figure 1). First, we discuss the fundamental principles of 2D c-MOFs within the context of gas sensor applications, encompassing their general properties, their proposed sensing mechanisms, and their integration into electrical devices. Subsequently, we provide a comprehensive summary of the reported 2D c-MOFs sensors, highlighting the various strategies employed to enhance their sensing performance. These strategies include the design of metal nodes and linkers, the control of morphology, and the utilization of composites based on 2D c-MOFs. We discuss how these approaches contribute to enhanced sensing characteristics of 2D c-MOFs sensors. Finally, we outline the prospects of 2D c-MOFs sensors and their potential for further advancement as highly effective sensing materials.

2. BASIC PRINCIPLES IN 2D C-MOFS CHEMIRESISTORS

2.1. Structural and Electrical Properties

Two key features of 2D c-MOFs are their well-defined porous frameworks and high electrical conductivities.[58] The porous structures are directly related to the sensing properties of 2D c-MOFs as they affect the mass transport of gases.[15,59] Meanwhile, high electrical conductivity is beneficial for operating chemiresistors with lower power consumption, particularly at room temperature.[60] The direct correlation between electrical conductivity and sensing characteristics has not been clearly established. However, several studies have indicated that 2D c-MOFs with lower conductivity may offer advantages in improving response.[61,62]

Both the porous structures and electrical properties of 2D c-MOFs can be tailored by selecting different linkers. Figure 2a−d and Table 1 show the lattice layers and conductivities of representative 2D c-MOFs with various linkers.[63−90] One notable difference is the pore sizes, which depend on the sizes of the linker molecules. For instance, triphenylene-based (HXTP) 2D c-MOFs exhibit larger honeycomb pores compared to benzene-based 2D c-MOFs (Figure 2a and c).

https://doi.org/10.1021/acsnanoscienceau.3c00024
ACS Nanosci. Au 2023, 3, 353−374

Table 1. Summary of Conductivities of Representative 2D c-MOFs[a]

2D c-MOFs	linker core, heteroatom	sample type	measurement method	conductivity (S/cm)	ref
$Cu_3(THQ)_2$	benzene, O	pellet	van der Pauw	7.3×10^{-8}	75
$Cu_3(HIB)_2$	benzene, N	pellet	van der Pauw	13	85
$Ni_3(HIB)_2$	benzene, N	pellet	van der Pauw	8	85
$Co_3(HIB)_2$	benzene, N	pellet	4-probe	1.57	67
$Ni_3(BHT)_2$	benzene, S	pellet	4-probe	2.8−160	90
$Pd_3(BHT)_2$	benzene, S	film	4-probe	0.028	84
$Cu_3(BHT)$	benzene, S	pellet	4-probe	48−280	83
		film	4-probe	2500	82
$Cu_3(HHTP)_2$	triphenylene, O	pellet	4-probe	0.02	86
		film	4-probe	0.29	81
		nanorod (sc[b])	4-probe	1.5	87
		nanoflake (sc)	2-probe	0.5	87
Ni−HHTP ($Ni_9(HHTP)_4$)	triphenylene, O	pellet	4-probe	0.01	80
		film	van der Pauw	1.1×10^{-3}	79
Co−HHTP ($Co_9(HHTP)_4$)	triphenylene, O	pellet	van der Pauw	0.032	79
		film	van der Pauw	3.3×10^{-3}	79
$Cu_3(HITP)_2$	triphenylene, N	pellet	4-probe	0.75	88
$Ni_3(HITP)_2$	triphenylene, N	pellet	4-probe	55.4	88
		film	van der Pauw	40	68
		nanorod (sc)	4-probe	150	87
$Co_3(HITP)_2$	triphenylene, N	pellet	4-probe	0.024	88
$Fe_3(HTTP)_2$	triphenylene, S	film	van der Pauw	0.2	78
$Co_3(HTTP)_2$	triphenylene, S	pellet	van der Pauw	1.4×10^{-3}	77
		film	van der Pauw	0.032	77
$Pt_3(HTTP)_2$	triphenylene, S	pellet	2-probe	3.86×10^{-6}	72
NiPc−Cu	phthalocyanine, O	pellet	4-probe	0.014	60
NiPc−Ni	phthalocyanine, O	pellet	4-probe	7.2×10^{-4}	60
CuPc−Cu	phthalocyanine, O	pellet	2-probe	9.4×10^{-8}−1.6×10^{-6}	76
NiIPc−Ni	phthalocyanine, N	film	4-probe	0.2	69
CuIPc−Ni	phthalocyanine, N	pellet	van der Pauw	1×10^{-4}	71

[a]This table presents selected examples of reported conductivities. Measured conductivity of the same 2D c-MOF can vary by 1−3 orders of magnitude across studies, depending on synthetic conditions, measurement methods, atmospheres, and other factors. [b]Conductivity of a single crystal.

In contrast, $Cu_3(BHT)$ exhibits a nonporous structure that may hinder the diffusion of gases within the frameworks (Figure 2b). However, 2D c-MOFs with shorter linkers can possess a higher density of active sites, which enables enhanced interactions with gases. In terms of electrical properties, describing the influence of linkers in a straightforward manner is challenging due to the complexity of the various factors involved. These factors include the length of pi conjugation, symmetry, density, and oxidation state, all of which can affect the conductivity of 2D c-MOFs.[22] One potential contributing factor is the type of heteroatom in the M−X linkage, which results in different degrees of π−d orbital overlap with the metals. The high degree of orbital overlap can contribute to improving charge mobility and narrowing band gap, thereby enhancing the conductivity of 2D c-MOFs.[58] For instance, $Cu_3(BHT)$ exhibits an ultrahigh conductivity of approximately 2500 S/cm with metallic behavior, owing to the high π−d orbital overlap of the M−S bond.[82] Meanwhile, metal nodes have a lesser influence on the overall structures of 2D c-MOFs compared to linkers. However, they can still significantly affect the electronic structures through their different capabilities to form orbital hybridizations with linkers. For example, the $M_3(HITP)_2$ series exhibits different band gaps (0.291−0.762 eV) and conductivities (5.8×10^{-3}−55 S/cm) depending on the choice of Cu, Co, and Ni nodes (Figure 2e).[88]

In addition to the 2D structures of layers, the stacking arrangement of the layers also plays a significant role in determining their structural and electrical properties. While 2D c-MOFs have been designed based on in-plane charge transport through extended conjugation pathways, recent studies have highlighted the importance of the out-of-plane pathway involving interlayer π−π stacking interactions.[87] This pathway has been found to make a significant contribution comparable to the in-plane pathway. Consequently, 2D c-MOFs with shorter interlayer spacing generally exhibit higher conductivity due to enhanced π−π overlap.[91] Moreover, different stacking patterns can be observed within the same layer, which includes eclipsed, serrated, and inclined arrangements (Figure 2f).[92] These distinct stacking patterns result in variations in porosity and electrical properties. For example, in 2D c-MOFs with highly staggered arrangements, the pores can be completely blocked by adjacent layers.[93] Additionally, some 2D c-MOFs are composed of two distinct layers with alternative stacking. A notable example is Co−HHTP, which consists of discrete molecular complexes integrated within the extended framework (Figure 2g and h). These discrete complexes possess different chemical structures and oxidation states compared to the extended layer, which can influence their activity toward guest molecules. Thus, considering the three-dimensional arrangement of the stacked layers is essential for gaining a comprehensive understanding of the structural

https://doi.org/10.1021/acsnanoscienceau.3c00024
ACS Nanosci. Au 2023, 3, 353−374

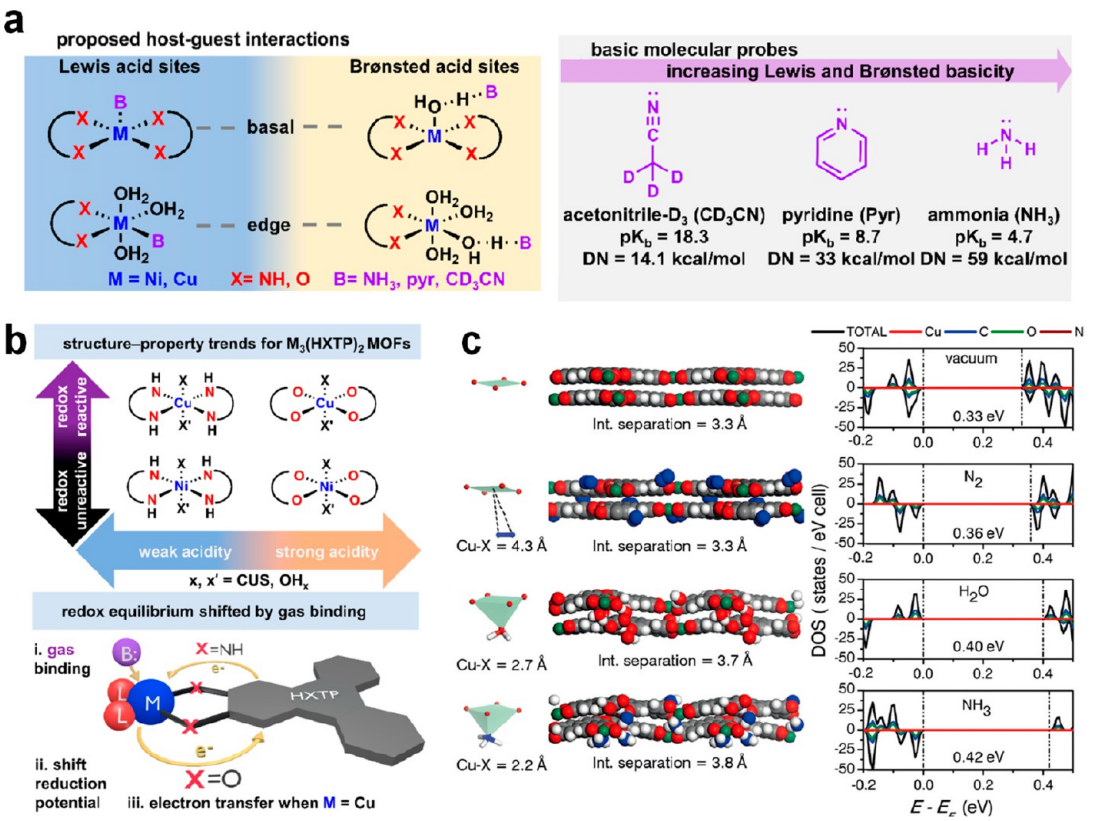

Figure 3. (a) Possible interactions of metal nodes in $M_3(HHTP)_2$ and $M_3(HITP)_2$ (M = Cu and Ni) with basic molecular probes. (b) The trend in redox activities and acidities of $M_3(HHTP)_2$ and $M_3(HITP)_2$. Adapted with permission from ref 95. Copyright 2020 American Chemical Society. (c) DFT-optimized structures and density of states of $Cu_3(HHTP)_2$ interacting with N_2, H_2O, and NH_3. Reprinted with permission from ref 94. Copyright 2019 Wiley-VCH.

and functional characteristics of 2D c-MOFs. Meanwhile, there are other 2D c-MOFs based on different linkers which are not described in this review.[56,58] Although their sensing characteristics have not been extensively investigated, they all hold great potential as promising candidates for implementing diverse features into gas sensors.

2.2. Gas Sensing Mechanisms

As 2D c-MOFs are relatively new sensing materials with a wide range of structures, their underlying sensing mechanisms have not been clearly established. However, identifying potential gas binding sites can serve as an initial step toward understanding the mechanism of these materials. In a general sense, metal nodes of 2D c-MOFs can be considered as highly active sites for gas binding. Rubio-Giménez et al. confirmed the coordination of NH_3 gas on metal nodes through both density functional theory (DFT) calculations and infrared spectroscopy.[94] The Mirica research group conducted an extensive study on the interaction of probe gases (NH_3, CD_3CN, pyridine) with metal complexes in $M_3(HITP)_2$ and $M_3(HHTP)_2$ (M = Cu and Ni) (Figure 3a).[95] They proposed that the metal sites can function as Lewis acid sites by directly accepting lone pairs from gases. These metal sites also can act as Brønsted acid sites through the mediation of hydrated H_2O ligands. Diffuse reflectance infrared Fourier transform spectroscopy (DRIFT) analysis revealed that the metal sites of all MOFs (MO_4 and MN_4) serve as Lewis acid sites to bind NH_3. Upon exposure to less basic gases (CD_3CN, pyridine), it was revealed that the Lewis acidity of HHTP-linked MO_4 sites is higher than that of HITP-linked MN_4 sites. Furthermore, the presence of NH_4^+ in the spectra of $M_3(HHTP)_2$ indicates that MO_4 complexes can also act as Brønsted acid sites simultaneously. In addition, metal sites in 2D c-MOFs can also function as catalytic sites, facilitating the transformation of gases into other species. For example, Ni nodes can oxidize adsorbed H_2S to sulfite or sulfate.[96] Although irreversible transformations can facilitate strong interactions with analytes, they often lead to irreversible sensing behavior.

In addition to gas binding on metal nodes, linkers in 2D c-MOFs can also serve as potential binding sites. Their various heteroatoms, such as O, N, and S, interact with a wide range of gases through hydrogen bonding or polar interaction. For example, Campbell et al. reported opposite sensing responses of $Cu_3(HITP)_2$ toward different amines ($^nBuNH_2$ and Et_3N), which is unusual in other sensing materials.[97] Considering the different hydrogen bonding capabilities of the secondary and tertiary amines, this implies that −NH moieties in the linker can interact with gases via hydrogen bonds.

Notably, the binding properties of metal nodes and linkers further vary depending on their location within a 2D c-MOF. For instance, the axial position of a metal node within the interior frameworks may not be accessible to gases due to the narrow interlayer spacing (~0.3 nm) of 2D c-MOFs. On the other hand, metal nodes located at the basal plane and the terminal edge are more accessible to gases.[95] The different coordination environments of the metal nodes lead to distinct chemical properties and binding behaviors. Therefore, understanding and controlling these distinct metal sites within 2D c-MOFs are crucial to optimize their sensing performance.

https://doi.org/10.1021/acsnanoscienceau.3c00024
ACS Nanosci. Au 2023, 3, 353−374

In chemiresistive response, the binding of analytes needs to be transduced into an electrical signal. One straightforward example is the change in charge density of the sensing materials caused by the exposure of the reducing or oxidizing gases. This change in charge density affects the electrical conductivity of the material, resulting in a measurable variation in its resistance. The charge transfer mechanism is also partially valid for 2D c-MOF sensors.[97,98] However, unusual sensing behaviors have been observed in 2D c-MOFs, suggesting that charge transfer alone is insufficient to explain their sensing mechanisms. In a study by the Mirica group, the oxidation state change of 2D c-MOFs after binding NH_3 was investigated using X-ray photoelectron spectroscopy (XPS) and electron paramagnetic resonance (EPR) analyses.[95] The results showed that the redox-active Cu nodes underwent oxidation or reduction upon analyte binding, but the overall frameworks of the MOFs maintained charge neutrality. Instead, the linker molecules were found to be reduced or oxidized to counterbalance the oxidation state change of the metal nodes (Figure 3b). The change in the oxidation state of the redox-active linker in 2D c-MOFs can lead to conductivity change through the generation of radicals or alterations in π−d hybridization.[22] On the other hand, despite the clear binding of NH_3, such redox events do not occur with Ni nodes since the stable oxidation state of Ni^{2+} is maintained.

In addition, the structural distortion of 2D c-MOFs upon binding gases can influence their electrical properties. Rubio-Giménez et al. observed that the binding of guest molecules led to the disruption of metal complexes and an increase in the interlayer spacing, which is related to out-of-plane charge transport (Figure 3c).[94] These changes in interlayer spacing were correlated with changes in conductivity induced by the guest molecules (N_2, H_2O, and NH_3). It is important to note that these mechanisms and other factors can simultaneously affect the electrical properties of 2D c-MOFs. The complex nature of the 2D c-MOFs, combined with the diverse binding sites of MOFs, poses challenges in elucidating the precise sensing mechanisms and designing optimal sensors. However, the distinctive sensing behavior of 2D c-MOFs, which is not observed in other sensing materials, holds immense potential for advancements in sensor technology.

2.3. Sensing Parameters and Related Design Principles

The performance of sensors upon interaction with target analytes can be effectively accessed by evaluating several key sensing parameters. First, the response can be defined by calculating normalized resistance (R) change upon exposure of analytes according to eq 1, where R_0 represents the baseline resistance observed under balance gas, and R_{gas} represents the resistance measured under gas exposure.

$$\text{response} = (R_{gas} - R_0)/R_0 = \Delta R/R_0 \quad (1)$$

In addition, the response also can be defined in terms of current (I) or conductance (G) from eq 2.

$$\text{response} = (I_{gas} - I_0)/I_0 = \Delta I/I_0 = \Delta G/G_0 \quad (2)$$

The response value is indeed a crucial parameter for comparing the performance of sensors. However, it should be noted that the two definitions of response, conductivity and resistivity, are not equivalent due to the inverse relationship between them. Also, the type of balance gas, which affects R_0 and the adsorption of analytes, should be considered when comparing the response. As a similar parameter, sensitivity (S) represents the ability of sensors to detect small changes in gas concentration. It is calculated from the slope (dy/dx) in the response (y) vs concentration (x) curve. The response and sensitivity of 2D c-MOFs can be influenced by factors such as surface area, number of binding sites, and gas accessibility. A higher surface area allows for enhanced surface interaction between the 2D c-MOFs and the analyte, promoting increased adsorption and improved sensor response. The number of binding sites available in the sensing material directly affects the capacity for interaction with the analyte, thereby impacting the response of the sensor. Furthermore, the accessibility of the gas molecules to the binding sites within the 2D c-MOFs can influence the response, as restricted or limited access may hinder effective sensing. Considering these factors is crucial for optimizing the performance of 2D c-MOFs as chemiresistive sensors. These factors can be further tailored in 2D c-MOFs through the selection of suitable linkers and control of morphology.

The response and recovery speeds are also crucial parameters for determining the performance of gas sensors. The response time (t_{res}) refers to the duration required for the sensor's response to dynamically reach 90% of the maximum response during exposure to the target gas. On the other hand, the recovery time (t_{rec}) is the time taken for the signal to return to 10% of the maximum response after the gas has been purged. In the case of 2D c-MOFs, sluggish response and recovery times are common issues due to their numerous binding sites and the operation of sensors at room temperature. However, these issues can be addressed through appropriate design strategies. One approach is to optimize the porous structure of the 2D c-MOFs to facilitate efficient gas diffusion and enhance the interaction with analyte molecules. Furthermore, the utilization of catalysts within the 2D c-MOFs can also accelerate the response and recovery speeds by promoting the desired chemical reactions involved in the sensing process. Another straightforward solution is to activate sensors using external stimuli. In conventional sensing materials like metal oxides, thermal activation through heating facilitates gas adsorption/desorption kinetics. However, this may not be suitable for MOFs-based sensors due to the relatively low thermal stability of MOFs. In this context, activation by light can be an excellent alternative to enhance the sensing speed of 2D c-MOFs sensors. Notably, 2D c-MOFs have narrower optical bandgaps (<1 eV) compared to insulating 3D MOFs, enabling efficient absorption of photon energy under visible light.[88,94,99,100]

Lastly, selectivity is a fundamental parameter that characterizes the ability of sensors to distinguish the target gas from other interfering gases. It is typically evaluated by comparing the response of the target gas to the responses of different analytes at a specific concentration.

As previously mentioned, one of the distinctive characteristics of 2D c-MOFs is the presence of diverse binding sites for target gases. This property provides opportunities to control and manipulate the interactions between the analytes and the MOF structure. Although the exact mechanism of the interaction is not well-understood, precise control of the composition of metal nodes and organic linkers can potentially lead to the tuning of selectivity across different MOFs.

2.4. Fabrication in Electronic Devices

Solvothermal synthesis is a versatile and essential approach for preparing a wide range of 2D c-MOFs specifically designed for

https://doi.org/10.1021/acsnanoscienceau.3c00024
ACS Nanosci. Au 2023, 3, 353−374

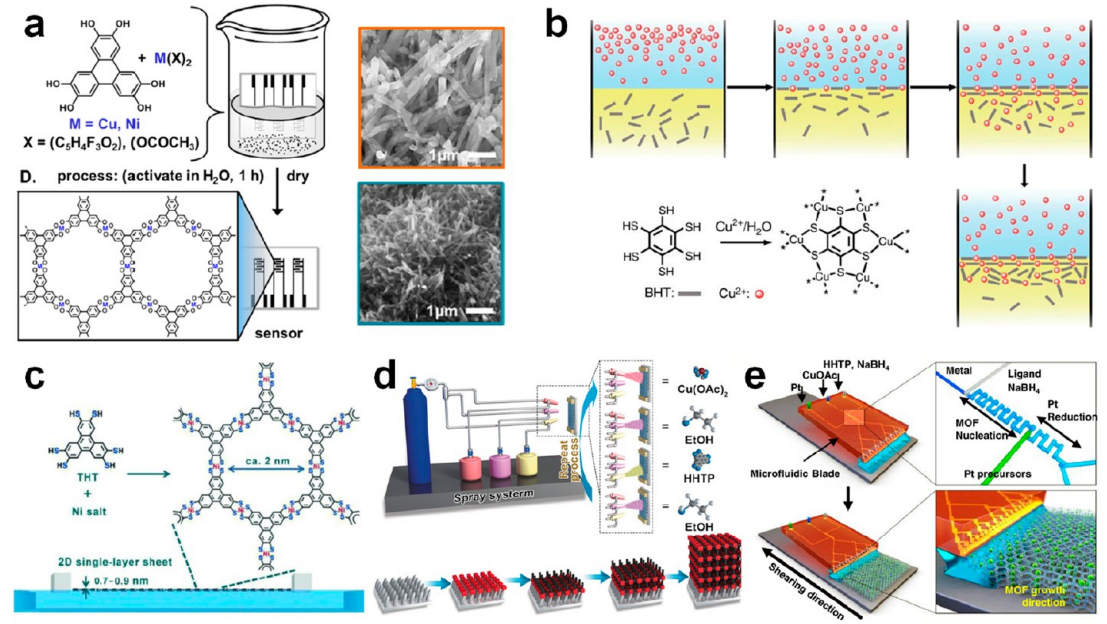

Figure 4. (a) Direct growth of $M_3(HHTP)_2$ polymer film. Reprinted with permission from ref 101. Copyright 2016 American Chemical Society (b) Synthesis of $Cu_3(BHT)$ at the liquid−liquid interface. Reprinted with permission under a Creative Commons CC BY License from ref 24. Copyright 2015 Springer Nature. (c) Synthesis of $Ni_3(HTTP)_2$ at the air−water interface assisted by the Langmuir−Blodgett method. Reprinted with permission from ref 103. Copyright 2015 Wiley-VCH. (d) Schematic illustration for the LBL assembly technique combined with spray-coating. Reprinted with permission from ref 98. Copyright 2017 Wiley-VCH. (e) Schematic illustration for the microfluidic channel-embedded solution shearing method. Reprinted with permission under a Creative Commons CC BY License from ref 104. Copyright 2021 Springer Nature.

sensor devices. By controlling the solvothermal conditions or postsynthetic treatment, the size and shape of the 2D c-MOFs can be modulated, which in turn affects their interaction with gases. Detailed discussions regarding the specific methods for controlling morphology and their impact on gas sensing performance will be discussed in a subsequent section. Through the utilization of ex situ coating methods, such as drop-casting, spray-coating, and mechanical abrasion, sensing devices can be fabricated from the as-synthesized 2D c-MOFs. Since the film fabrication process is independent of MOF synthesis conditions, these methods allow for a wide range of 2D c-MOFs to be employed. However, these methods often result in poor adhesion and contact with substrate and/or electrode. Moreover, there is a risk of sample damage during preparation, which can impede the reproducible sensing measurements.[57] Alternatively, 2D c-MOFs can be directly grown on a suitable substrate under solvothermal synthetic conditions (Figure 4a).[101,102] The direct growth approaches generally enhance contact of devices and minimize damage to the samples. Nonetheless, achieving precise control over the thickness or orientation of the film is challenging in solvothermal synthesis.

To achieve more precise control over film fabrication, the liquid interfacial synthesis method can be employed.[89] This approach allows the synthesis of 2D c-MOFs within a confined space at the interface, resulting in films with controlled thickness and orientation. For instance, Huang et al. demonstrated the synthesis of $Cu_3(BHT)$ at the interface of dichloromethane and water, where the linker and Cu precursors were dissolved separately (Figure 4b).[24] The resulting $Cu_3(BHT)$ film exhibited controlled thickness (10−140 nm), with layers arranged in a parallel orientation. Another method for obtaining thin films of 2D c-MOFs is the Langmuir−Blodgett-assisted technique, which enables the formation of monolayers at the air−liquid interface (Figure 4c).[103] In this process, ligands are spread over the liquid surface and compressed to form a dense monolayer. By introducing metal precursors onto the surface, monolayers of 2D c-MOFs can be synthesized. The films prepared at the liquid interface can be easily transferred onto sensing substrates.

Alternatively, a layer-by-layer (LBL) approach allows for the direct deposition of thin films of 2D c-MOFs on functionalized surfaces (Figure 4d).[98] By repeated coating of linker and ligand layers, MOFs can be grown layer by layer with precise control over thickness (<2 nm per cycle). Another technique, microfluidic-based solution shearing, enables the large-area synthesis of very thin and uniform films of 2D c-MOFs on substrates (Figure 4e).[104] In this method, MOF precursors are rapidly mixed and reacted within a microfluidic-channel embedded blade. The shearing of the blade facilitates controlled growth of the MOF from the reaction mixture at the edge of the meniscus (liquid−air interface). The thickness of the resulting thin film can be precisely controlled up to tens of nanometers by adjusting the shearing speed of the blade. While these thin-film fabrication methods require rather sophisticated techniques or specialized equipment, their high level of controllability over the growth of 2D c-MOFs offers advantages in developing high-performance and reliable sensing devices.

3. APPLICATIONS AND STRATEGIES IN CHEMIRESISTORS

3.1. Design and Selection of Metal Modes and Linkers

As mentioned above, the high structural tunability of MOFs is one of their key advantages as sensing materials. The diverse

https://doi.org/10.1021/acsnanoscienceau.3c00024
ACS Nanosci. Au 2023, 3, 353−374

Table 2. Summary of the Sensing Properties of 2D c-MOF Sensors Based on the Design of Metal Nodes and Linkers

sensing material	response type	response	target gas	operating condition	ref
$Cu_3(HITP)_2$	$\Delta G/G_0$	2.6%@10 ppm	NH_3	N_2, r.t.	105
$Cu_3(HHTP)_2$	$\Delta I/I_0$	0.7%@80 ppm	NH_3	N_2, r.t.	101
	$\Delta I/I_0$	−1.8%@80 ppm	NO	N_2, r.t.	
	$\Delta I/I_0$	0.5%@80 ppm	H_2S	N_2, r.t.	
$Ni_3(HHTP)_2$	$\Delta I/I_0$	−1.7%@80 ppm	NO	N_2, r.t.	101
	$\Delta I/I_0$	4.2%@80 ppm	H_2S	N_2, r.t.	
$Ni_3(HHTP)_2$ on cotton	$-\Delta G/G_0$	−49%@80 ppm	NO	N_2, r.t.	102
	$-\Delta G/G_0$	98%@80 ppm	H_2S	N_2, r.t.	
$Ni_3(HITP)_2$ on cotton	$-\Delta G/G_0$	81%@80 ppm	NO	N_2, r.t.	102
	$-\Delta G/G_0$	97%@80 ppm	H_2S	N_2, r.t.	
0.1 mol % HITP doped Cu-HHTP	$\Delta R/R_0$	240%@100 ppm	NH_3	air, r.t	62
10 mol % HITP doped Cu-HHTP	$\Delta R/R_0$	90%@100 ppm	benzene	air, r.t	62
Cu-HHTP-THQ	$\Delta I/I_0$	21.6%@100 ppm	NH_3	air, r.t.	61
Cu-THQ	$\Delta I/I_0$	63.5%@100 ppm	NH_3	air, r.t	61
$Cu_3(HIB)_2$	S ($\Delta G/G_0$)	$-0.62\%\ (100\ ppm)^{-1}$	CO_2	80 RH% air, r.t.	107
CoPc−Cu	$-\Delta G/G_0$	27.4%@80 ppm	CO	N_2, r.t	108
NiPc−Cu	$-\Delta G/G_0$	18.9%@80 ppm	CO	N_2, r.t	108
NiPc−Ni	$-\Delta G/G_0$	43%@80 ppm	NH_3	N_2, r.t.	60
	$-\Delta G/G_0$	64%@80 ppm	H_2S	N_2, r.t.	
	$-\Delta G/G_0$	−657%@1 ppm	NO	N_2, r.t.	
NiPc−Cu	$-\Delta G/G_0$	45%@80 ppm	NH_3	N_2, r.t.	60
	$-\Delta G/G_0$	98%@80 ppm	H_2S	N_2, r.t.	
	$-\Delta G/G_0$	−397%@1 ppm	NO	N_2, r.t.	
2D Cu−salphen-MOF	$\Delta I/I_0$	766%@100 ppm	NO_2	Air, r.t	109

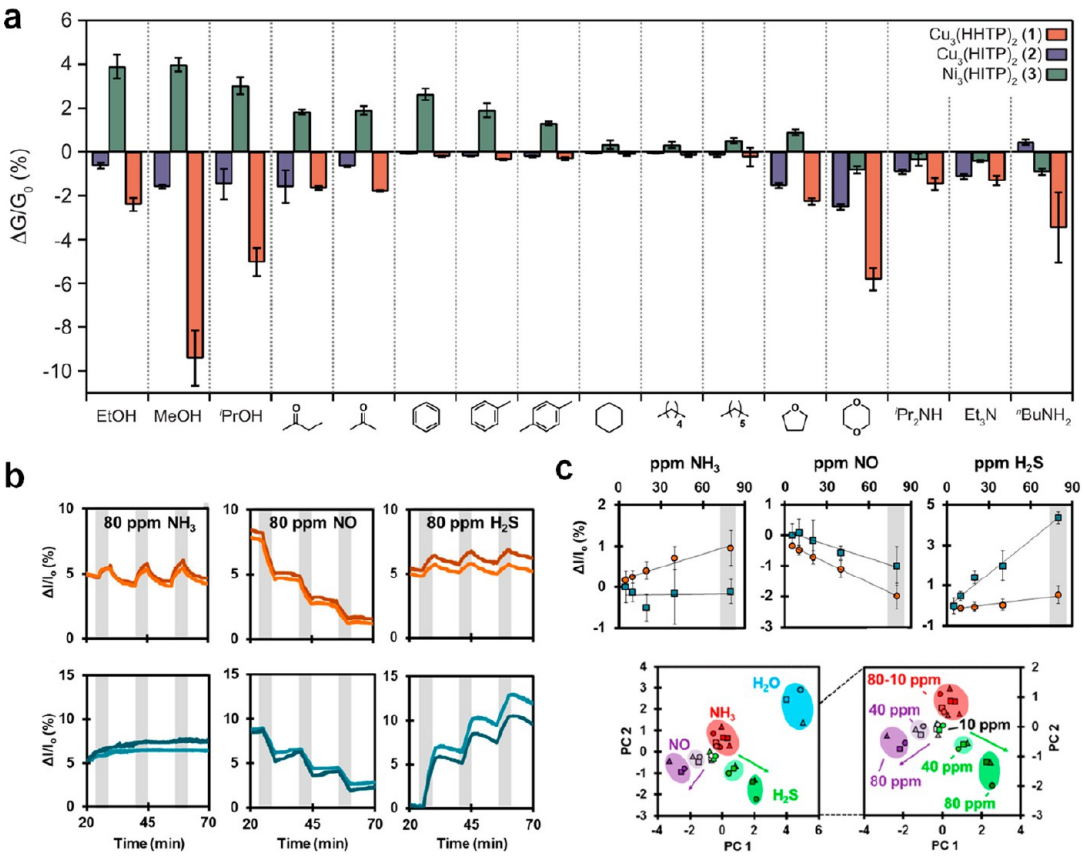

Figure 5. (a) Sensing responses of the MOF array to representative examples from different categories of VOCs. Reprinted with permission from ref 97. Copyright 2015 American Chemical Society. (b) Sensing traces of $Cu_3(HHTP)_2$ (orange) and $Ni_3(HTTP)_2$ (blue) toward 80 ppm of NH_3, NO, and H_2S. (c) Sensing responses of $Cu_3(HHTP)_2$ and $Ni_3(HTTP)_2$ with different concentrations of NH_3, NO, and H_2S and their principal component analysis results. Adapted with permission from ref 101. Copyright 2016 American Chemical Society.

https://doi.org/10.1021/acsnanoscienceau.3c00024
ACS Nanosci. Au 2023, 3, 353−374

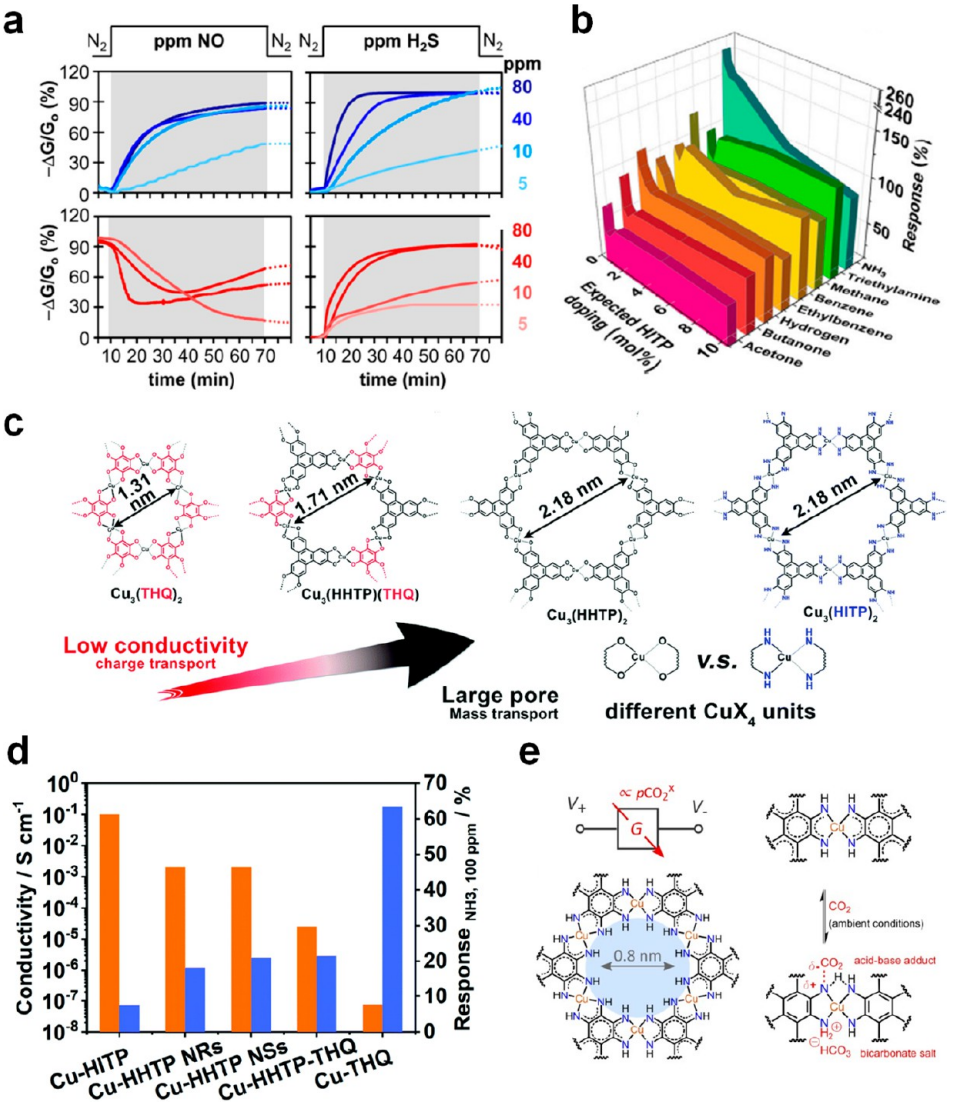

Figure 6. (a) Sensing traces of $Ni_3(HITP)_2$ (blue) and $Ni_3(HHTP)_2$ (red) toward NO and H_2S. Reprinted with permission from ref 102. Copyright 2017 American Chemical Society. (b) The selectivity chart of Cu-HHTP with different doping concentrations of HITP. Reprinted with permission from ref 62. Copyright 2021 Springer Nature Group. (c) Structures of isostructural 2D c-MOFs with THQ, HHTP, and HITP organic ligands. (d) Comparison of conductivities and the response values of the isostructural 2D c-MOFs. Reprinted with permission from ref 61. Copyright 2021 Royal Society of Chemistry. (e) Schematic illustration of $Cu_3(HIB)_2$ for CO_2 sensing. Reprinted with permission from ref 107. Copyright 2019 American Chemical Society.

chemical properties arising from numerous combinations of organic linkers and metal nodes determine the interaction of MOFs with analytes. Although the exact mechanisms underlying these interactions have not been clearly elucidated, selecting or designing nodes and linkers should be the primary strategy to achieve the desired sensing performance. In this section, we introduce how different nodes or linkers affect the sensing properties of 2D c-MOFs and related strategies to further improve sensing performance based on their properties. The sensing performances of 2D c-MOF sensors with different nodes and linkers are summarized in Table 2.

3.1.1. Tuning Metal Nodes. Metal nodes of 2D c-MOFs are commonly regarded as the most likely binding sites for analytes. These metal nodes often have coordination sites that can interact with target gases, leading to selective sensing capabilities. Therefore, changing nodes with different metals significantly affects the sensing behavior of 2D c-MOFs. Campbell et al. first reported 2D c-MOF-based chemiresistors using $Cu_3(HITP)_2$ and $Ni_3(HITP)_2$, which are composed of the same linker but different metals.[105] $Cu_3(HITP)_2$ exhibited increased conductance ($\Delta G/G_0$ = 2.6%) upon exposure to 10 ppm of NH_3, while $Ni_3(HITP)_2$ showed no significant response toward NH_3. This result is consistent with the study conducted by the Mirica group, which proposed that redox-active Cu nodes are responsible for the electronic interaction with NH_3, while inactive Ni nodes do not exhibit such interaction.[95] Campbell et al. further investigated the different sensing behaviors of these MOFs toward 16 other VOCs (aliphatic/aromatic hydrocarbons, alcohols, ketones, and amines).[97] $Cu_3(HITP)_2$ and $Ni_3(HITP)_2$ exhibited opposite changes in conductance toward most of the targets (Figure 5a). Considering that the charge transfer mechanism plays a crucial role in chemiresistive sensors, these results imply that the different charge densities associated with metal nodes (e.g., d^8 Ni^{II} vs d^9 Cu^{II}) can have a substantial impact on the sensing response toward a wide range of targets. Similar

https://doi.org/10.1021/acsnanoscienceau.3c00024
ACS Nanosci. Au 2023, 3, 353−374

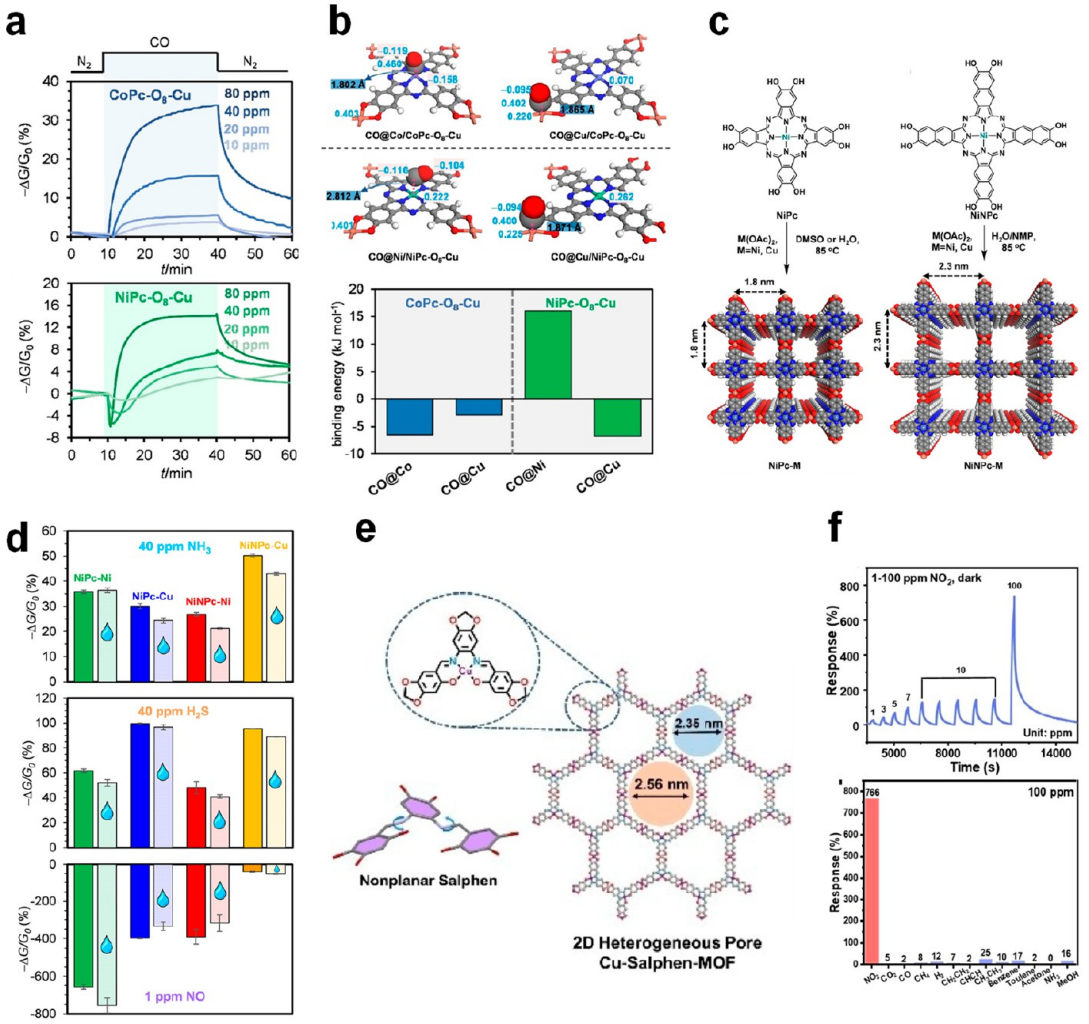

Figure 7. (a) Sensing traces of CoPc−Cu and NiPc−Cu upon exposure to 80−10 ppm of CO. (b) DFT-optimized structure of CO-adsorbed CoPc−Cu and NiPc−Cu and their binding energies. Reprinted with permission from ref 108. Copyright 2022 Wiley-VCH. (c) Synthetic scheme for isoreticular phthalocyanine and naphthalocyanine-based MOFs, NiPc−M, and NiNPc−M. (d) Sensing responses of NiPc−M and NiNPc−M MOFs to 40 ppm of NH_3, 40 ppm of H_2S, and 1 ppm of NO in dry nitrogen and in the presence of 5000 ppm of H_2O. Reprinted with permission from ref 60. Copyright 2019 American Chemical Society. (e) The structure of nonplanar salphen and Cu−salphen-MOF. (f) Response of Cu−salphen-MOF toward NO and other 11 types of gases (100 ppm). Reprinted with permission from ref 109. Copyright 2023 Wiley-VCH.

behaviors are observed for 2D c-MOFs based on the HHTP linker, the same triphenylene core with −OH groups. While $Cu_3(HHTP)_2$ sensors showed a positive conductance change to 80 ppm of NH_3, the Ni counterparts exhibited no significant response (Figure 5b).[101] Moreover, it is worth noting that more than two different nodes can be simultaneously incorporated in isoreticular 2D c-MOFs. By mixing and controlling the compositions of Cu, Ni, and Co nodes in $M_3M'_{3-x}(HITP)_2$, continuous variation of the electrical conductivity over 6 orders of magnitude can be achieved.[88] Although the sensing properties of these bimetallic MOFs have not been studied, this approach offers an additional option for fine-tuning the sensing characteristics of 2D c-MOFs.

Besides, the 2D c-MOF sensors with altered cross-sensitivities depending on the choice of nodes can be combined into an array to more precisely discriminate multiple gases. For example, an array of Ni− and Cu−HHTP-based sensors can differentiate 10−80 ppm of NO, NH_3, and H_2S using principal component analysis (PCA), which is known as one of the pattern recognition approaches (Figure 5c).[101] However, it should be noted that the selection of the node is not solely responsible for the sensing characteristics of 2D c-MOFs and may not always result in different sensitivity. For example, all Cu−, Co−, Ni−, and Fe−HHTP-based sensors exhibited similar responses toward NO.[86]

3.1.2. Controlling Organic Linkers. Linkers, as another main component of 2D c-MOFs, also play a crucial role in influencing sensing properties. Similar to the case of changing metal nodes, substituting the linker with different heteroatoms can lead to contrasting responses in gas sensing behavior. For example, $Ni_3(HITP)_2$ exhibits a negative conductance change ($\Delta G/G_0$ = −81%) in response to 80 ppm of NO, which is opposite to its HHTP counterpart ($\Delta G/G_0$ = 49%) (Figure 6a).[102] The opposing behaviors may arise from linker-dependent variations in different charge carrier types (p or n) or ligand-specific interactions with analytes (−OH and $-NH_2$). The different activity of 2D c-MOFs with different linkers, often combined with the "tuning nodes" approach, can further enhance gas discrimination capabilities through PCA. Additionally, the combination of isostructural ligands in 2D c-MOFs offers the ability to further tune sensor performance. Wu et al. demonstrated this interesting feature by creating a

https://doi.org/10.1021/acsnanoscienceau.3c00024
ACS Nanosci. Au 2023, 3, 353−374

dual-ligand Cu-HHTP/HITP thin film with a doping level of approximately up to 10 mol % HITP.[62] By controlling the doping concentration of HITP, cross-sensitivity between various gases (amines, benzenes, hydrogen, and ketones) was gradually modulated (Figure 6b). Notably, the 10 mol% HITP-doped Cu-HHTP exhibited a higher response to 100 ppm of benzene ($\Delta R/R_0$ = 90%) compared to NH_3 ($\Delta R/R_0$ = 80%), which contrasts with the selectivity observed in the 0.1 mol % HITP-doped counterpart ($\Delta R/R_0$ = 75% to benzene and 240% to NH_3). This reversed selectivity is intriguing since typical 2D c-MOF sensors are more sensitive to highly reducing NH_3 compared to nonpolar VOCs. The authors proposed that the n-type doping effect of HITP reduces the sensitivity toward electron-donating reducing gases. They also suggested that the interaction of abundant defects formed by HITP doping have influenced the selectivity of the 2D c-MOF sensors.

Furthermore, two structurally distinct ligands also can be mixed to develop a new structure of 2D c-MOFs. The Kitagawa research group successfully synthesized Cu−HHTP−THQ by hybridizing HHTP (molecular size: 0.97 nm) and much smaller THQ (tetrahydroxy-1,4-quinone, molecular size: 0.55 nm).[61,106] Cu−HHTP−THQ has a moderate pore size (1.71 nm) and electrical conductivity (2.53×10^{-5} S/cm), intermediate to that of Cu−HHTP and Cu−THQ. With high porosity and moderate conductivity, Cu−HHTP−THQ showed high sensitivity and linearity toward NH_3 concentrations below 100 ppm. Furthermore, a comparative study on Cu−THQ, Cu−HHTP−THQ, Cu−HHTP, and Cu−HITP was conducted to investigate the influence of linker-dependent properties on sensing performance (Figure 6c).[61] A negative relationship was observed between electrical conductivity of 2D c-MOF and their sensing response toward 100 ppm of NH_3. This suggests that 2D c-MOF with lower intrinsic conductivity may exhibit higher sensitivity to charge transfer from low-concentration gases (Figure 6d). Additionally, the different porous structures of the MOFs influenced the sensing kinetics. $Cu_3(THQ)_2$, with the smallest 1D honeycomb pore size (1.31 nm), showed much slower reaction and recovery speeds compared to other MOFs with larger pores (1.71−2.18 nm), attributable to sluggish gas diffusion through the small 1D pores. However, sensing speeds of the 2D c-MOFs with larger pores were found to be influenced by the overall pore volume (including interparticle pores and other mesopores determined by morphologies) rather than solely relying on the size of the honeycomb pores.

Ligands with a benzene core, such as THQ, represent the smallest linker units in 2D c-MOFs. Their subnanoporous structure may hinder the mass transport of large analytes and limit the uptake of high gas concentrations. However, their relatively dense structures are advantageous as gas sensors in certain aspects. Stassen et al. reported CO_2 sensors using $Cu_3(HIB)_2$ based on acid−base interaction between CO_2 and amines in HIB (Figure 6e).[107] Due to the small size of HIB, $Cu_3(HIB)_2$ can have a high density of amine groups serving as gas binding sites, while the pore size is large enough (0.8 nm) to allow CO_2 molecules to access the pores. Accordingly, $Cu_3(HIB)_2$ exhibited a sensitivity of −0.62% $(100\ ppm)^{-1}$, which is higher than the analogous $Cu_3(HITP)_2$ with a lower density of amine groups and even comparable to commercial nondispersive infrared (NDIR) sensors. Furthermore, the nanopores of $Cu_3(HIB)_2$ can be fully hydrated even at very low humidity levels (∼10% RH). Owing to this unique property, $Cu_3(HIB)_2$-based sensors can effectively minimize the effect of humidity, maintaining an invariant CO_2 response above 10% RH. These characteristics set $Cu_3(HIB)_2$-based sensors apart from other sensors that are unable to maintain such invariant CO_2 response in humid conditions.

3.1.3. Metallolinker-Based 2D c-MOFs. Recently, metallophthalocyanines (MPc) have been utilized to synthesize high-performance chemiresistors in the form of 2D c-MOFs. One notable characteristic of MPc-based 2D c-MOFs is that the linkers themselves contain metal sites, which increases the diversity of 2D c-MOFs and provides additional gas binding sites for intriguing sensing properties. The Mirica research group demonstrated the utility of these additional metal sites in MPc-based 2D c-MOFs for gas sensing.[108] They synthesized CoPc−Cu and NiPc−Cu by connecting the Cu node with Co- or Ni-centered MPc. CoPc−Cu exhibited an enhanced response toward CO ($-\Delta G/G_0$ = 27.4%) compared to that of analogous NiPc−Cu ($-\Delta G/G_0$ = 18.9%) (Figure 7a). Furthermore, CoPc−Cu had a much lower detection limit (0.53 ppm) compared to NiPc−Cu (3.0 ppm). DRIFTS analysis indicated that Cu nodes were primarily responsible for CO binding in both 2D c-MOFs. However, the DFT calculation revealed that the Co sites serve as stable binding sites for CO (ΔE = −6.5 kJ/mol), which is comparable to Cu sites. On the other hand, the Ni sites are found to be unfavorable for CO binding (ΔE = 16.0 kJ/mol) (Figure 7b). This suggests that the metal center in MPc can serve as a secondary interaction site to further modulate the sensing response. In addition to changing the metal center, substituting the node and linker in isoreticular MPc-based 2D c-MOFs also contributes to the tuning of sensing properties. Meng et al. investigated the sensing properties of analogous MOFs with the combinations of Cu/Ni nodes with NiPc- and Ni-centered naphthalocyanine (NiNPc) linkers (Figure 7c).[60] Intriguingly, different combinations of nodes and linkers resulted in noticeable variations in sensitivity, selectivity, kinetics, and reversibility toward NO, H_2S, and NH_3 (Figure 7d), respectively. For instance, NiPc-based MOFs exhibited higher responses to NO compared to NiNPc, and the Cu node was more efficient in detecting H_2S than Ni.

Metallosalphen is a new type of metallolinker that can be utilized to construct 2D c-MOFs (Figure 7e).[109] While typical 2D c-MOFs are synthesized from planar ligands, salphen has a nonplanar structure. However, salphen can be converted into a planar configuration through the coordination of a metal ion within its N_2O_2 pocket. In addition, six ortho-substituted hydroxyl groups are coordinated simultaneously to metal ions, forming a unique structure of 2D c-MOFs. The Cu−salphen MOF, owing to the additional Cu coordination in salphen, possesses two distinct Cu sites ($Cu-N_2O_2$ and $Cu-O_4$) with higher metal density compared to typical 2D c-MOFs. Cu−salphen MOF exhibited a remarkably high response ($\Delta I/I_0$ = 786% to 100 ppm of NO_2), which can be attributable to the high density of Cu sites (Figure 7f). DFT and XPS analyses have revealed that the unique $Cu-N_2O_4$ sites are particularly responsible for the high activity toward NO_2.

3.2. Morphology Control

2D c-MOFs possess diverse gas binding sites that exhibit varying activity toward target gases. Furthermore, their anisotropic crystal structure leads to different chemical/electrical properties and gas diffusivities depending on their orientations. Hence, manipulating the morphology of 2D c-MOFs can result in significant differences in sensitivity,

https://doi.org/10.1021/acsnanoscienceau.3c00024
ACS Nanosci. Au 2023, 3, 353−374

selectivity, and reaction dynamics. In this section, we introduce several interesting approaches for controlling the morphology including crystal growth control and thin-film fabrication, with the aim of improving gas sensing characteristics. Table 3 provides a summary of various 2D c-MOF sensors associated with morphological manipulation techniques.

Table 3. Summary of the Sensing Properties of 2D c-MOF Sensors with the Morphology Control Strategy

sensing material	response type	response	target gas	operating condition	ref
$Cu_3(HHTP)_2$ nanoflakes	$\Delta R/R_0$	89.4%@ 5 ppm	NO_2	air, r.t	99
crystalline $Ni_3(HIB)_2$	$\Delta I/I_0$	0.8@80% RH	H_2O	N_2, r.t	111
amorphous $Ni_3(HIB)_2$	$\Delta I/I_0$	45@80% RH	H_2O	N_2, r.t	111
$Cu_3(BHT)$ film	$\Delta R/R_0$	14.9%@ 100 ppm	NH_3	air, r.t	112
$Cu_3(HHTP)_2$ film with LBL process	$\Delta R/R_0$	129%@ 100 ppm	NH_3	air, r.t.	98
$Cu_3(HHTP)_2$-3C (3 LBL cycles)	$\Delta I/I_0$	55.9%@ 100 ppm	NH_3	air, r.t	113
	$\Delta I/I_0$	9.1%@ 100 ppm	H_2	air, r.t	
$Cu_3(HHTP)_2$-5C	$\Delta I/I_0$	197.6%@ 100 ppm	NH_3	air, r.t	113
	$\Delta I/I_0$	65%@ 100 ppm	H_2	air, r.t	
$Cu_3(HHTP)_2$-20C	$\Delta I/I_0$	133.9%@ 100 ppm	NH_3	air, r.t	113
	$\Delta I/I_0$	66.3%@ 100 ppm	H_2	air, r.t	
$Cu_3(HHTP)_2$ 3D thin film	$\Delta R/R_0$	161%@ 100 ppm	NH_3	air, r.t	114
$Ni_3(HITP)_2$ thin film	$\Delta R/R_0$	2085%@ 5 ppm	H_2S	N_2, r.t	115

3.2.1. Control of Crystal Shape and Crystallinity. Reducing the size of crystallites is a universal strategy for enhancing sensitivity in gas sensing. Smaller crystal size provides advantages such as increased gas accessibility and effective surface area. Jo et al. investigated the effect of the crystal size of $Cu_3(HHTP)_2$ on its response to NO_2.[99] The sizes of $Cu_3(HHTP)_2$ nanoflakes were controlled by collecting the supernatant after centrifugation at different speeds (50−5000 rpm). The response gradually increased from 61.1% to 89.4% toward 5 ppm of NO_2 as the particle size increased from 158 to 415 nm (Figure 8a). Yao et al. reported similar observations for the response of $Cu_3(HHTP)_2$ to NH_3.[61] In this case, $Cu_3(HHTP)_2$ nanosheets were synthesized by controlling the reaction conditions such as the solvent and precursor concentrations. $Cu_3(HHTP)_2$ nanosheets exhibited higher response and faster responding speed compared to rod-shaped counterparts synthesized under typical solvothermal conditions. This difference is attributed to the shorter diffusion length in the *c*-axis of nanosheets. Another useful approach for controlling crystal shape is the addition of a coordination modulator during synthesis. For example, the addition of ammonia during synthesis suppresses the growth of $Cu_3(HHTP)_2$ in the *c*-axis, resulting in nanoplatelets with a thickness of approximately 10 nm.[110] The $Cu_3(HHTP)_2$ nanoplatelets can be spray-coated on a substrate with parallel orientation, further increasing the accessibility of 1D pores. The sensing devices fabricated from the spray-coating of nanoplatelets exhibited an immediate resistance change ($\Delta R/R_0$ = 140%) in response to MeOH.

Moreover, reducing crystallinity and generating defects can also be advantageous in gas sensing as it creates binding sites with higher activity. Liu et al. synthesized Ni−HIB by partially oxidizing hexaaminobenzene linkers (HIB) to pentaaminobenzene or tetraaminobenzene.[111] The resulting Ni−HIB synthesized from the oxidized linkers contained numerous missing-linker defects, leading to a loss of crystallinity (Figure 8b). The Ni−HIB with missing-linker defects showed a much higher response and fast responding speed ($\Delta I/I_0$ = 45, t_{res} = 4.92 s) compared to crystalline $Ni_3(HIB)_2$ ($\Delta I/I_0$ = 0.8, t_{res} = 36.77 s) toward H_2O (80% relative humidity) (Figure 8c). This high activity is attributed to the hydroxyl group substituted at the missing-linker sites, which facilitates interaction with water molecules through hydrogen bonding. In addition, Chen et al. reported an increase in response of $Cu_3(BHT)$ with low crystallinity.[112] During the synthesis of the $Cu_3(BHT)$ film, it was observed that reducing the reaction time led to the formation of less crystalline sample with an increased number of defective Cu sites on the surface of the crystals (Figure 8d). The authors observed a synergistic relationship between the NH_3 response and the number of defective Cu sites (Figure 8e). Through DFT analysis, it was revealed that the defective Cu sites are responsible for the high responses by providing strong binding energy toward NH_3.

3.2.2. Fabrication of Thin Film. Fabricating sensing materials in thin-film form is a straightforward approach that promotes gas diffusion and improves sensitivity. The Xu research group developed a method for constructing thin films of 2D c-MOFs using a LBL assembly technique combined with spray-coating.[98] By employing LBL processes, $Cu_3(HHTP)_2$ thin films were successfully fabricated with high orientation, excellent crystallinity, and well-controlled thickness ranging from 20 to 100 nm. The $Cu_3(HHTP)_2$ thin film exhibited a resistance change of 129% toward 100 ppm of NH_3, which is 5 times higher than that of the powder-based thick-film sensor (Figure 9a). Additionally, the thin-film sensors exhibited faster gas diffusion rate compared to a powder-based sensor, with response and recovery speeds increased by 54% and 10%, respectively. In a subsequent study, the Xu group further investigated the LBL growth process of thin films and its impact on sensing properties (Figure 9b).[113] During the initial few growth cycles, in-plane growth of grains was self-limited to sizes below 40 nm. The low crystallinity of the films was self-repaired after 10 cycles. Consequently, the responses of the thin film toward H_2 and NH_3 significantly increased between 5 and 10 growth cycles, reflecting the formation of a charge transport pathway for sensing signal transduction. Beyond the 10th cycle, the response toward NH_3 decreased due to reduced mass transport in thicker film. However, this effect had a lesser impact on H_2 due to its smaller kinetic diameter. Furthermore, the thin film can also be grown on a 3D substrate with the LBL process to further enhance the exposed surface area, leading to improved mass transport.[114] Lin et al. successfully fabricated a 3D $Cu_3(HHTP)_2$ thin film on a substrate consisting of TiO_2 nanowire arrays (Figure 9c).[114] The 3D thin-film-based sensor exhibited a 2.5 times higher response and a 2.3 times faster responding speed compared to the 2D thin-film sensor (Figure 9d).

Lee et al. demonstrated the fabrication of $Ni_3(HITP)_2$ thin-film sensors using microfluidic-assisted solution shearing and postsynthetic crystallization techniques (Figure 9e).[115] Ini-

https://doi.org/10.1021/acsnanoscienceau.3c00024
ACS Nanosci. Au 2023, 3, 353−374

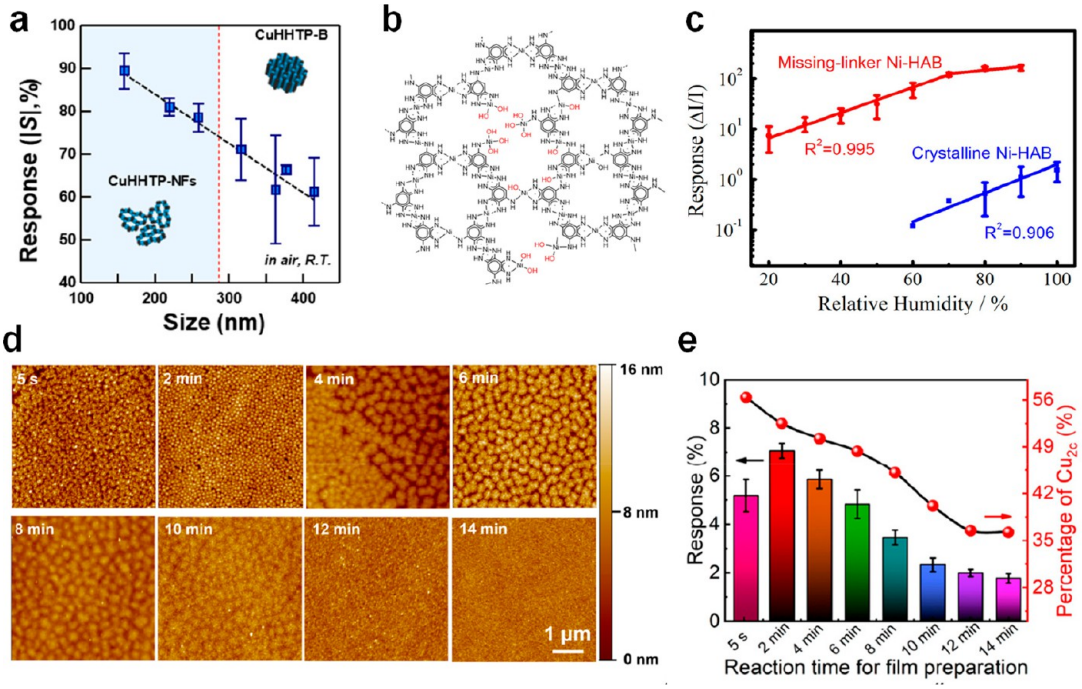

Figure 8. (a) Sensing responses for bulk and nanoflakes of $Cu_3(HHTP)_2$. Reprinted with permission under a Creative Commons CC BY-NC-ND License from ref 99. Copyright 2021 American Chemical Society. (b) Structure of amorphous $Ni_3(HIB)_2$ with missing-linker sites. (c) Humidity sensing responses of missing-linker $Ni_3(HIB)_2$ (Ni−HAB in the figure) and crystalline $Ni_3(HIB)_2$. Reprinted with permission from ref 111. Copyright 2021 American Chemical Society. (d) Surface morphologies of $Cu_3(BHT)$ film with different reaction times for film preparation. (e) Reaction-time-dependent NH_3 response (bar chart) and Cu_{2c} percentage (red dotted line) of $Cu_3(BHT)$ films. Reprinted with permission from ref 112. Copyright 2020 American Chemical Society.

tially, thin films of precrystallized $Ni_3(HITP)_2$ were formed through solution shearing, with precise control over the film thickness ranging from 11 to 64 nm. Subsequent amine treatment was applied to induce deprotonation of the linker, resulting in rapid crystallization of ∼30 nm crystallites with parallel orientation in the thin film. The $Ni_3(HITP)_2$ thin film exhibited a significantly higher response to H_2S, with a 30-fold increase compared to the powder-based sensor (Figure 9f). The enhanced sensitivity can be attributed to the thin-film structure, parallel orientation, and uniform nanocrystallites achieved during the fabrication process.

3.3. Composites of 2D c-MOFs

Combining sensing materials with other materials is a well-known strategy for tuning the sensing properties. This approach can be highly effective for 2D c-MOFs, especially considering the incomplete understanding of their sensing mechanisms. By incorporating 2D c-MOFs with other materials whose effects on gases are relatively predictable, a more rational option can be provided for tuning the sensing characteristics in a desired manner, rather than directly modifying the 2D c-MOFs themselves. In this section, we present several examples of foreign materials in 2D c-MOF composites, along with their effects on sensing performance. The sensing performances of 2D c-MOF composite sensors are summarized in Table 4.

3.3.1. Decoration of Nanoparticles. Various metal nanoparticles (NPs) have been employed as effective sensitizers in gas sensors, which activate sensing materials chemically or electronically.[116] MOFs are especially advantageous for the strategy due to their cavities for stabilizing NPs.[117−119] Koo et al. utilized this concept to combine NPs and $Cu_3(HHTP)_2$ for application in highly sensitive NO_2 gas sensors.[120] The well-defined porous structure of $Cu_3(HHTP)_2$ enables confined growth of ultrasmall Pt or Pd NPs (<2 nm) with high dispersity (Figure 10a). The responses of Pt@$Cu_3(HHTP)_2$ ($\Delta R/R_0$ = −57.38%) and Pd@$Cu_3(HHTP)_2$ (−62.11%) toward 5 ppm of NO_2 are higher than that of pristine $Cu_3(HHTP)_2$ (−29.95%). In more detail, the Pt and Pd NPs affected the response in a distinct mechanism. Pt@$Cu_3(HHTP)_2$ exhibited a lower activation energy for the adsorption of NO_2, implying that Pt acts as a chemical sensitizer through the spillover effect. Meanwhile, Pd acts as an electronic sensitizer in Pd@$Cu_3(HHTP)_2$. NO_2 adsorption and charge transfer on Pd lower the Schottky barrier between NPs and $Cu_3(HHTP)_2$, resulting in an amplified signal (Figure 10b). Using similar approaches, Sun et al. reported the sensitization of $Co_3(HITP)_2$ by incorporating Pd, Au, and Pt NPs for highly sensitive H_2S sensors.[121] In addition, the NPs@2D-c-MOFs can be fabricated as thin films, resulting in further increased sensitivity. Kim et al. demonstrated the fabrication of Pt@$Cu_3(HHTP)_2$ thin films using in situ growth by microfluidic channel-embedded solution shearing.[104] The Pt@$Cu_3(HHTP)_2$ thin film exhibited a higher response ($\Delta R/R_0$ = −89.9% to 3 ppm of NO_2) compared to both the $Cu_3(HHTP)_2$ thin film and $Cu_3(HHTP)_2$ powder-based thick film (Figure 10c).

Furthermore, the use of bimetallic nanoparticles, which exhibit higher activity due to the synergistic effect between two different metal elements, can further enhance sensing performance. Dipolar interactions and site-specific growth of two different metals within the cavities of 2D c-MOFs allow the facile synthesis of ultrasmall bimetallic NPs, which is challenging in typical synthetic methods.[122] $Cu_3(HHTP)_2$ with bimetallic PtRu NPs showed an enhanced response

https://doi.org/10.1021/acsnanoscienceau.3c00024
ACS Nanosci. Au 2023, 3, 353−374

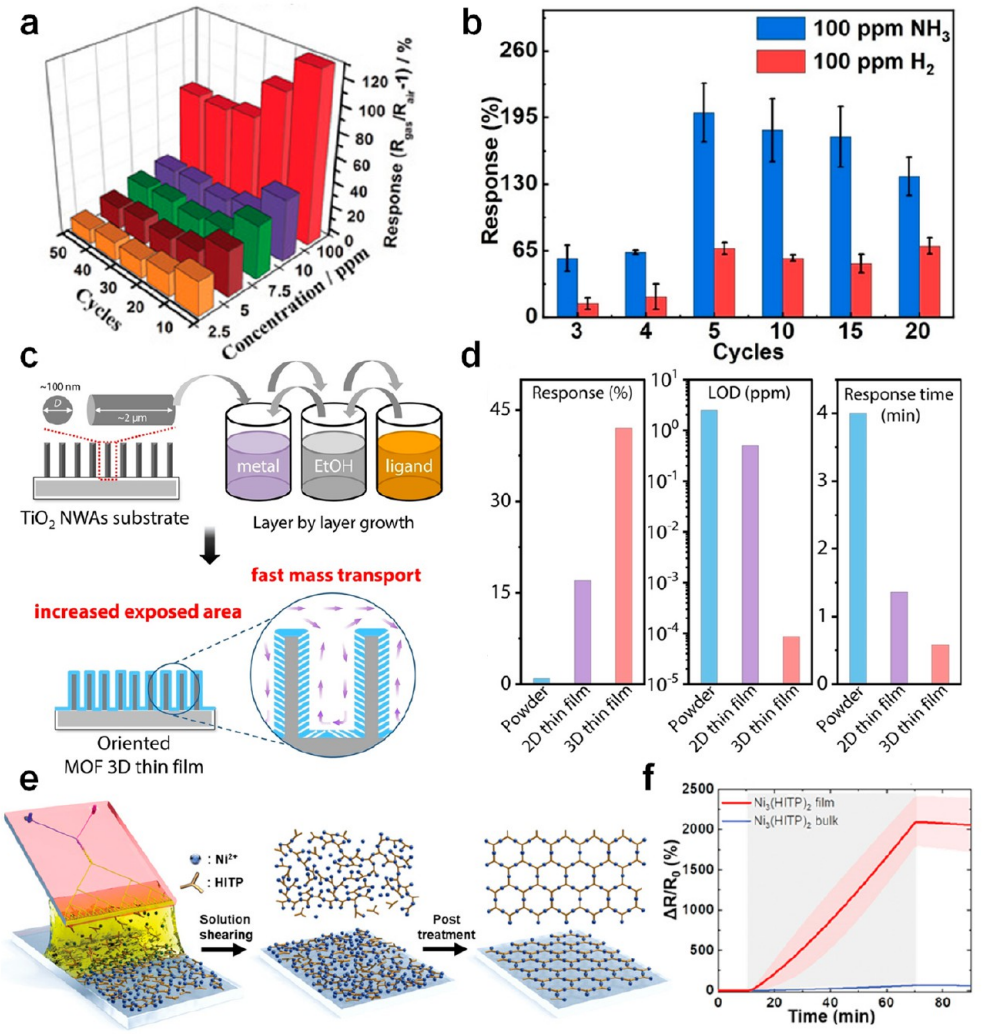

Figure 9. (a) NH_3 sensing responses of $Cu_3(HHTP)_2$ film with different LBL growth cycles. Reprinted with permission from ref 98. Copyright 2017 Wiley-VCH. (b) Growth-cycle-dependent responses of the $Cu_3(HHTP)_2$ film toward 100 ppm of NH_3 and H_2. Reprinted with permission from ref 113. Copyright 2022 Wiley-VCH. (c) Schematic illustration for fabrication of oriented MOF 3D thin film using the LBL assembly technique. (d) Sensing performance for powder, 2D thin film, and 3D thin film of $Cu_3(HHTP)_2$. Reprinted with permission from ref 114. Copyright 2021 Wiley-VCH. (e) The schematic figure for fabrication of $Ni_3(HITP)_2$ thin-film processing using the microfluidic-based solution shearing (f) Dynamic sensing trace of bulk and thin-film $Ni_3(HITP)_2$ toward 5 ppm of H_2S. Reprinted with permission from ref 115. Copyright 2022 Wiley-VCH.

($\Delta R/R_0$ = −53.0% to 2 ppm of NO_2) compared to its monometallic Pt and Ru counterparts (Figure 10d). The improved response of PtRu@$Cu_3(HHTP)_2$ originates from the synergistic combination of the spillover effect by Pt and strong gas adsorption on Ru. With this approach, a diverse range of sensitization effects can be designed based on the combination of two metals, leading to further control of sensing properties in NPs@2D c-MOFs.

Additionally, Jo et al. utilized a mixture of $Cu_3(HHTP)_2$ and Fe_2O_3 nanoparticles for the NO_2 sensor, focusing on reversibility.[99] Pristine $Cu_3(HHTP)_2$ exhibits high sensitivity and selectivity toward NO_2. However, the response toward NO_2 is not reversible due to the strong adsorption of NO_2, requiring additional activation for desorption. Light illumination on $Cu_3(HHTP)_2$ generates photogenerated holes to desorb $NO_2^-{}_{(ads)}$, enhancing reversibility at room temperature (Figure 10e). However, complete recovery cannot be achieved due to the fast recombination of photogenerated carriers before desorption. To address this issue, Fe_2O_3 nanoparticles (<50 nm) are decorated on $Cu_3(HHTP)_2$ by physical mixing, forming a heterojunction where photogenerated carriers can be separated with a longer lifetime. As a result, Fe_2O_3–$Cu_3(HHTP)_2$ exhibited completely reversible sensing behavior toward NO_2 under light illumination (Figure 10f).

3.3.2. Hybridization of Hydrophobic/Hydrophilic Materials. Modulating the surface hydrophobicity of sensors represents a rational approach for discriminating gases based on their polarity.[123] This strategy holds particular promise for 2D c-MOF-based sensors, which typically exhibit high sensitivity toward a limited range of highly polar molecules such as NH_3, H_2S, and NO_2, while their ability to discriminate less-polar VOCs remains underdeveloped. A convenient method to manipulate the polarity of 2D c-MOFs involves incorporating other materials with varying degrees of hydrophobicity. Wang et al. conducted a study on the polarity-dependent sensing properties of phthalocyanine-based MOFs

https://doi.org/10.1021/acsnanoscienceau.3c00024
ACS Nanosci. Au 2023, 3, 353−374

Table 4. Summary of the Sensing Properties of 2D c-MOF-Based Composite Sensors

sensing material	response type	response	target gas	operating condition	ref
$Cu_3(HHTP)_2$	$\Delta R/R_0$	−29.95%@5 ppm	NO_2	air, r.t.	120
$Pd@Cu_3(HHTP)_2$	$\Delta R/R_0$	−62.11%@5 ppm	NO_2	air, r.t.	120
$Pt@Cu_3(HHTP)_2$	$\Delta R/R_0$	−57.38%@5 ppm	NO_2	air, r.t.	120
$Co_3(HITP)_2$	R_{gas}/R_{air}	4.25@100 ppm	H_2S	air, r.t	121
$Au_2-Co_3(HITP)_2$	R_{gas}/R_{air}	5.10@100 ppm	H_2S	air, r.t	121
$Pd_2-Co_3(HITP)_2$	R_{gas}/R_{air}	8.08@100 ppm	H_2S	air, r.t	121
$Pt_2-Co_3(HITP)_2$	R_{gas}/R_{air}	6.38@100 ppm	H_2S	air, r.t	121
$Cu_3(HHTP)_2$ thin film	$\Delta R/R_0$	−53.7%@3 ppm	NO_2	air, r.t.	104
$Pt@Cu_3(HHTP)_2$ thin film	$\Delta R/R_0$	−89.9%@3 ppm	NO_2	air, r.t.	104
$PtRu@Cu_3(HHTP)_2$	$\Delta R/R_0$	−53.0%@2 ppm	NO_2	air, r.t	122
$Pt@Cu_3(HHTP)_2$	$\Delta R/R_0$	−39.6%@2 ppm	NO_2	air, r.t	122
$Ru@Cu_3(HHTP)_2$	$\Delta R/R_0$	−20.3%@2 ppm	NO_2	air, r.t	122
$Fe_2O_3-Cu_3(HHTP)_2$ nanoflakes	$\Delta R/R_0$	−64%@5 ppm	NO_2	air, light illumination	99
$Ni_2[CuPc(NH)_8]-OTMS$	$-\Delta G/G_0$	3.22%@400 ppm	MeOH	N_2, r.t	124
Cu−TCPP-on-Cu−HHTP	$\Delta R/R_0$	153%@100 ppm	benzene	air, r.t.	126
Ni−HHTP@UiO-66−NH_2	$\Delta R/R_0$	3.37@5 ppm	H_2S	air, r.t	129

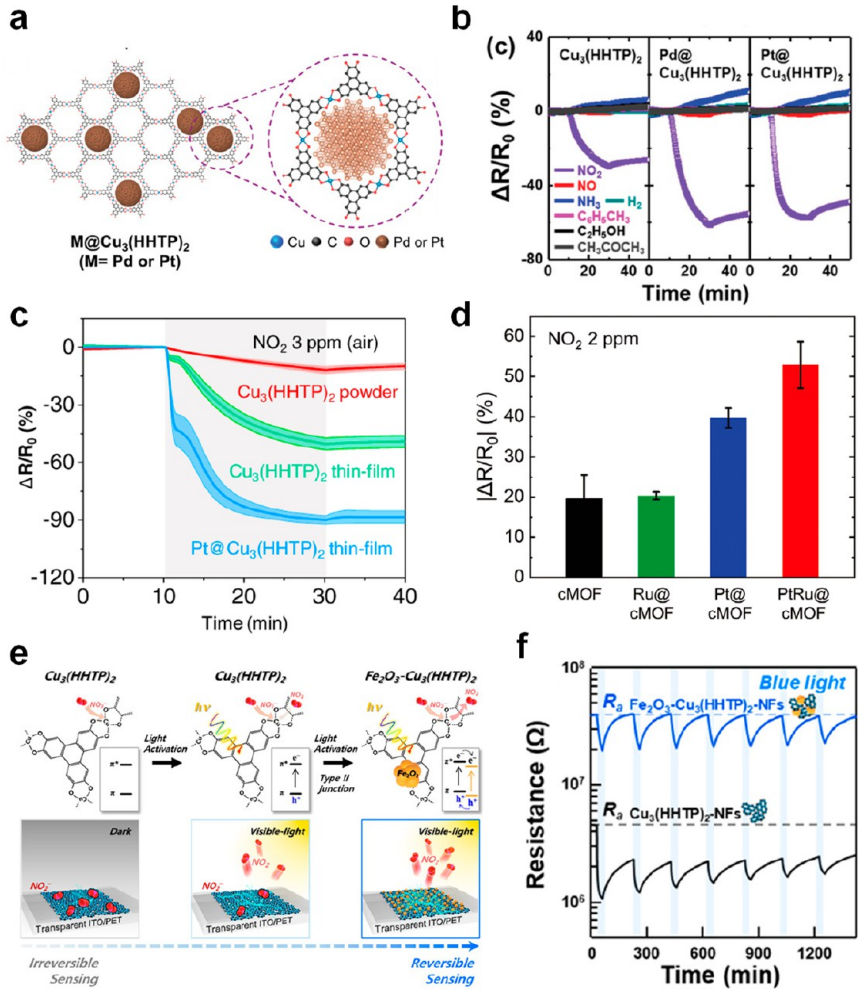

Figure 10. (a) Schematic illustration for nanoparticle encapsulation of $Cu_3(HHTP)_2$ (b) Selective gas sensing performance of $Cu_3(HHTP)_2$, $Pd@Cu_3(HHTP)_2$, and $Pt@Cu_3(HHTP)_2$. Reprinted with permission under a Creative Commons CC BY License from ref 120. Copyright 2019 Wiley-VCH. (c) Sensing performance for $Cu_3(HHTP)_2$ powder, thin film, and thin film with Pt decoration using microfluidic channel-embedded solution shearing. Reprinted with permission under a Creative Commons CC BY License from ref 104 . Copyright 2021 Springer Nature. (d) Sensing responses of Pt, Ru, and PtRu NP- encapsulated $Cu_3(HHTP)_2$ for 2 ppm of NO_2. Reprinted with permission from ref 122. Copyright 2021 Wiley-VCH. (e) Reversible NO_2 sensing mechanism of $Fe_2O_3-Cu_3(HHTP)_2$ using visible light. (f) Repetitive sensing traces of $Fe_2O_3-Cu_3(HHTP)_2$ and $Cu_3(HHTP)_2$ toward 5 ppm of NO_2 under blue light illumination. Reprinted with permission under a Creative Commons CC BY-NC-ND License from ref 99. Copyright 2021 American Chemical Society.

https://doi.org/10.1021/acsnanoscienceau.3c00024
ACS Nanosci. Au 2023, 3, 353−374

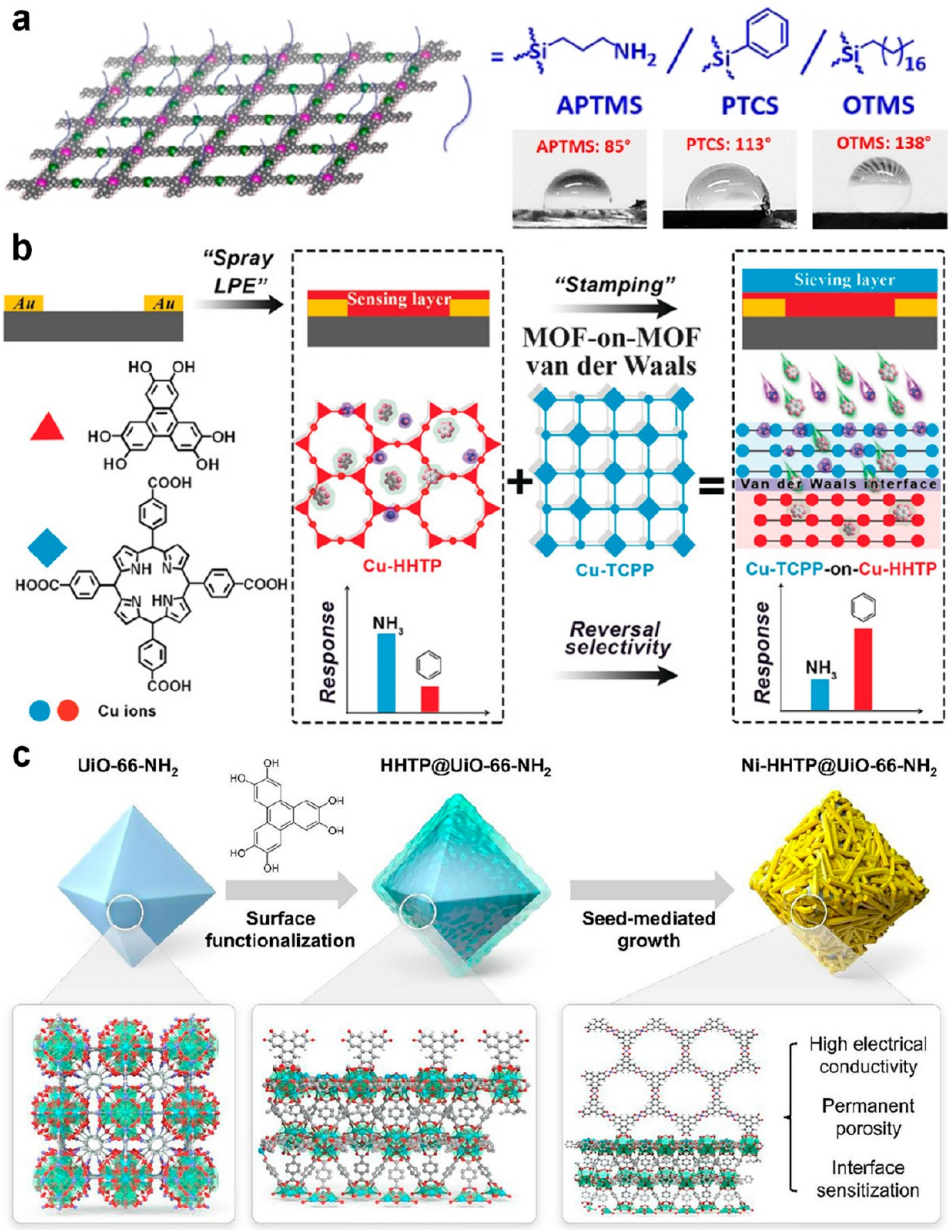

Figure 11. (a) Schematic illustration for surface-modification of $Ni_2[CuPc(NH)_8]$ 2D c-MOF film with APTMS, PTCS, and OTMS coating. Reprinted with permission from ref 124. Copyright 2021 Wiley-VCH. (b) Schematic illustration for the fabrication of MOF-on-MOF film. Reprinted with permission from ref 126. Copyright 2019 Wiley-VCH. (c) Schematic illustration for the synthesis of the heterostructured Ni–HHTP@UiO-66–NH_2. Reprinted with permission from ref 129. Copyright 2022 Elsevier.

($Ni_2[Cu(NHPc)]$) by coating the surface of the MOFs with silanes possessing different functional groups (Figure 11a).[124] Upon coating with octadecyltrimethoxysilane (OTMS), which features a long hydrophobic alkyl chain, the sensor exhibited a reduction in response (from $\Delta G/G_0$ = 4.7% to 1.7%) toward 600 ppm of H_2O, along with an enhanced recovery speed. This can be attributed to the suppression of water adsorption by the hydrophobic OTMS layer, consequently enabling faster desorption. The grafting of propylamine, a relatively hydrophilic moiety, had minimal impact on the H_2O sensing properties. Furthermore, OTMS-grafted 2D c-MOFs exhibited an enhanced response and recovery toward methanol compared to the pristine sample. They also observed a positive relationship between the response speeds and the polarity of the analytes (methanol > ethanol > isopropanol). Although the impact of OTMS on the sensing response to polar VOCs remains unclear and complex, their study offers additional opportunities for tuning the selectivity toward VOCs.

3.3.3. Integration with Other MOFs. As MOFs have various interactions with a wide range of gases, compositing 2D c-MOFs with other MOFs can offer intriguing sensing properties. One of the representative functions is the gas separation ability of MOFs which can be applied to modulate the selectivity of sensors.[125] Xu's group fabricated MOF-on-MOF film and demonstrated the selectivity tuning.[126] As a 2D c-MOF layer, $Cu_3(HHTP)_2$ thin film was prepared by the LBL process (Figure 11b). The $Cu_3(HHTP)_2$ film showed considerable response to benzene (134% to 100 ppm), but the response was weaker compared to the response to polar NH_3 (230% to 100 ppm). To reverse the selectivity, a Cu–

https://doi.org/10.1021/acsnanoscienceau.3c00024
ACS Nanosci. Au 2023, 3, 353–374

TCPP layer was transferred onto the $Cu_3(HHTP)_2$ thin film. The Cu−TCPP layer limited the permeation of NH_3 through strong binding at unsaturated Cu sites. Consequently, the Cu−TCPP-on-$Cu_3(HHTP)_2$ film showed a significantly reduced response to NH_3 (from 230% to 94%), while maintaining a similar level of response to benzene (from 134% to 153%). It is noteworthy that the Cu−TCPP layer was synthesized independently and coated onto the $Cu_3(HHTP)_2$ film, overcoming their structural dissimilarity with a van der Waals gap. This approach enables the incorporation of a diverse range of MOFs known for their gas separation capabilities, thereby imparting selectivity toward different gases.[127]

Furthermore, MOFs can be integrated via coordination bonds to exert stronger effects on each other.[128] Cho et al. synthesized a heterostructure of UiO-66−NH_2 and Ni−HHTP by connecting them through coordination bonds (Figure 11c).[129] The heterostructure was formed by initially synthesizing UiO-66−NH_2 crystallites as the core, followed by connecting HHTP linkers to the Zr nodes of UiO-66−NH_2. Subsequent growth of the Ni−HHTP shell resulted in well-connected core−shell heterostructures of the two MOFs. The heterostructured sensors exhibited a high surface area of 1071 m^2/g, which was close to the predicted value based on their composition and surface areas (449 m^2/g for Ni-HHTP and 1320 m^2/g for UiO-66−NH_2), indicating that the highly porous structures and numerous active sites of both MOFs were maintained in the heterostructures. Additionally, several unique properties were observed at the interface between the two MOFs. First, the interfacial coordination of HHTP at Zr nodes led to the formation of a high concentration of ligand-centered radicals, which are advantageous for redox reactions with analytes. Second, DFT calculations revealed that the highest occupied molecular orbital (HOMO) level was localized at the interfacial HHTP, enhancing the effectiveness of charge transfer between reducing gases. As a result, the Ni−HHTP@UiO-66−NH_2 exhibited a higher response to 5 ppm of H_2S ($\Delta R/R_0$ = 3.37) compared to pristine Ni−HHTP ($\Delta R/R_0$ = 0.71). Moreover, UiO-66−NH_2 in the heterostructure provided secondary binding sites for H_2S, facilitating its desorption more easily than in Ni−HHTP alone. Consequently, Ni−HHTP@UiO-66−NH_2 showed improved reversibility toward H_2S.

4. SUMMARY AND PERSPECTIVES

2D c-MOFs possess well-defined porous structures, high electrical conductivity, and numerous active sites. These features are highly tunable depending on the combination of metal nodes and linkers, making them unique materials in gas sensing applications. Their tunable pore sizes and densities of active sites impact the diffusion and adsorption of gases. Tailoring electrical properties of 2D c-MOFs can affect power consumption, signal noise, and potentially response of the sensors. In addition, the strategic combinations of nodes and linkers can give rise to various distinct binding characteristics, including Lewis or Brønsted acid, hydrogen bonding, and a range of other polar interactions. In addition, mechanisms underlying the conductivity changes are also diverse and complex. Along with charge transfer, unique conductivity-change mechanisms have been observed in 2D c-MOFs, such as the redox of linkers counterbalancing the charge shift in nodes and the disruption of interplanar interactions. Overall, the precise control and optimization of these unique properties of 2D c-MOFs hold significant potential for the development of high-performance gas sensors.

In this regard, various 2D c-MOFs-based devices have been demonstrated based on three approaches: (1) design and selection of linkers, (2) control of morphologies, (3) and integration of foreign materials with 2D c-MOFs. Among them, the design of metal nodes and linkers is the most crucial approach for determining the sensing properties of 2D c-MOFs. Controlling metal nodes significantly influences the binding affinity toward specific target gases as strong binding sites. They also affect the subsequent change in electrical signal through different redox activity or charge density. These differences lead to even contrasting responses toward certain targets. While linkers have similar influences, they determine the porous structure of 2D c-MOFs, affecting gas diffusivity and response speed. Meanwhile, metal-centered ligands further increase the chemical diversity by introducing additional metal sites. However, a large barrier in this strategy is the lack of a clear understanding of the relationship between chemical structures and sensing behaviors. To fully exploit the design potential of 2D c-MOFs, further investigations are needed to establish a comprehensive understanding of the intricate relationship between their structure and sensing properties. Alternatively, a more predictable approach involves the combination of two different nodes or linkers with finely tuned compositions. The mixed 2D c-MOFs may induce moderate properties that lie between those of the two pristine MOFs. However, the synthesis of such mixed 2D c-MOFs, especially those with linkers possessing different cores, poses a significant challenge. To overcome this challenge, innovative synthetic methods should be further developed.

The morphology control approach in 2D c-MOFs offers an additional pathway to achieve distinct properties without altering the nodes or linkers. By manipulating synthetic conditions or applying postsynthetic treatments, the shape and size of the crystals can be tuned. Smaller crystallites, particularly in the form of nanosheets, facilitate gas diffusion within the interior volume, making them advantageous for gas sensing. Reducing crystallinity and introducing defect sites can enhance the gas binding activity. However, these approaches sacrifice the electrical conductivities of the 2D c-MOFs, requiring careful optimization to balance the trade-off. Instead, through various techniques, the thickness of the 2D c-MOFs film can be reduced to <100 nm, significantly reducing the gas diffusion length. Some of these techniques (e.g., the LBL method) induce parallel orientation of the crystallites, further improving the accessibility of the pores and binding sites. The further development of the film fabrication techniques may enable the exploration of the orientation effect on other crystallographic planes (e.g., preferred exposure of edge sites) or different stacking patterns. Thus, thin-film 2D c-MOFs can provide additional functionality to the sensors. Additionally, efforts are being made to fabricate high-quality films with larger domains and fewer defects.[56] Although sensor studies reveal that contrasting properties (small crystallites and numerous defects) tend to be advantageous for higher sensing response, high-quality films may allow the deeper study of intrinsic conductivity changes in 2D c-MOFs and provide valuable insights into sensing mechanisms.

Hybridization of 2D c-MOFs with other well-defined selectors or catalysts offers a promising approach for the rational design of 2D c-MOFs chemiresistors, providing more predictability. For instance, metal or metal-oxide nanoparticles

https://doi.org/10.1021/acsnanoscienceau.3c00024
ACS Nanosci. Au 2023, 3, 353−374

can be integrated to utilize their well-known functions in gas sensors, such as chemical or electronic sensitizers. In addition, other materials with different polarities, surface charges, or acidities can be integrated to facilitate or inhibit gas adsorption. In particular, the decoration of metal nanoparticles has been widely employed in the field of gas sensors, and numerous prior studies have elucidated the sensing mechanisms of various metals. The well-defined pores of MOFs enable the incorporation of diverse metal nanoparticles. Despite these advantages and the extensive previous research, the decoration of metal nanoparticles in 2D c-MOF sensors has not been extensively studied, leaving significant room for exploring and enhancing the sensing characteristics of such composites. However, at the same time, the 1D pore channel of 2D c-MOFs is prone to pore blocking issues when nanoparticles are decorated on the surface. This approach inevitably compromises the porosity and surface reaction sites of 2D c-MOFs and requires careful optimization of the decoration method and loading amount of nanoparticles. To address this, other porous MOFs can be integrated as foreign materials, minimizing the pore blocking problem. These MOFs act as a sieving layer when arranged as a MOF-on-MOF structure, allowing the diffusion of target gases while effectively blocking interfering gases. Currently, the utilization of these MOF layers is primarily focused on filtering gases and controlling selectivity. However, they can also contribute to enhancing the sensitivity and response speed of sensors by harnessing other functionalities of MOFs, such as gas storage and preconcentration. In addition, MOFs can be integrated with stronger bonds, benefiting from the catalytic effects of adjacent MOFs and exploiting various intriguing interfacial properties. Relevant studies have shown that the sensitization effect of MOFs can be comparable to the decoration of catalytic nanoparticles. Although integrating structurally distinct MOFs and achieving strong coupling pose challenges, the construction of appropriate heterostructures can effectively overcome the surface blocking issue associated with conventional sensitizers in gas sensing applications.

Despite the existing challenges and the need for further advancements, the utilization of 2D c-MOFs holds immense promise in addressing current limitations in gas sensors. While there is still a significant gap in achieving the desired sensing properties, we believe that the rapid development of this emerging material class will play a pivotal role in the functionalization of next-generation conducting MOF-based chemiresistors in the near future.

AUTHOR INFORMATION

Corresponding Author

Il-Doo Kim − *Department of Materials Science and Engineering, Korea Advanced Institute of Science and Technology (KAIST), Yuseong-gu, Daejeon 34141, Republic of Korea*; orcid.org/0000-0002-9970-2218; Email: idkim@kaist.ac.kr

Authors

Chungseong Park − *Department of Materials Science and Engineering, Korea Advanced Institute of Science and Technology (KAIST), Yuseong-gu, Daejeon 34141, Republic of Korea*

Jong Won Baek − *Department of Materials Science and Engineering, Korea Advanced Institute of Science and Technology (KAIST), Yuseong-gu, Daejeon 34141, Republic of Korea*

Euichul Shin − *Department of Materials Science and Engineering, Korea Advanced Institute of Science and Technology (KAIST), Yuseong-gu, Daejeon 34141, Republic of Korea*

Complete contact information is available at: https://pubs.acs.org/10.1021/acsnanoscienceau.3c00024

Author Contributions

All the authors take full responsibility for the content of this review and approved its submission. CRediT: **Chungseong Park** writing-original draft (lead), writing-review & editing (lead); **Jong Won Baek** writing-original draft (supporting), writing-review & editing (supporting); **Euichul Shin** writing-original draft (supporting), writing-review & editing (supporting).

Notes

The authors declare no competing financial interest.

ACKNOWLEDGMENTS

This work was supported by Korea Technology and Information Promotion Agency for SMEs (Grant No. 00141845) and the National Research Foundation of Korea (NRF) grant funded by the Korea government, Ministry of Science and ICT (Development of Ultra-High Density Nanofibers Yarn Based Multi-Modal Gas Sensor Platform) (Grant No. 2020R1A2C301312712).

REFERENCES

(1) Daglar, H.; Gulbalkan, H. C.; Avci, G.; Aksu, G. O.; Altundal, O. F.; Altintas, C.; Erucar, I.; Keskin, S. Effect of metal-organic framework (MOF) database selection on the assessment of gas storage and separation potentials of MOFs. *Angew. Chem., Int. Ed.* **2021**, *60*, 7828−7837.

(2) Chen, Z.; Kirlikovali, K. O.; Idrees, K. B.; Wasson, M. C.; Farha, O. K. Porous materials for hydrogen storage. *Chem.* **2022**, *8*, 693−716.

(3) Sharma, A.; Lim, J.; Lah, M. S. Strategies for designing metal-organic frameworks with superprotonic conductivity. *Coord. Chem. Rev.* **2023**, *479*, 214995.

(4) Liu, J.; Goetjen, T. A.; Wang, Q.; Knapp, J. G.; Wasson, M. C.; Yang, Y.; Syed, Z. H.; Delferro, M.; Notestein, J. M.; Farha, O. K.; Hupp, J. T. MOF-enabled confinement and related effects for chemical catalyst presentation and utilization. *Chem. Soc. Rev.* **2022**, *51*, 1045−1097.

(5) Li, Z.; Gao, R.; Feng, M.; Deng, Y. P.; Xiao, D.; Zheng, Y.; Zhao, Z.; Luo, D.; Liu, Y.; Zhang, Z.; Wang, D.; Li, Q.; Li, H.; Wang, X.; Chen, Z. Modulating metal-organic frameworks as advanced oxygen electrocatalysts. *Adv. Energy Mater.* **2021**, *11*, 2003291.

(6) Yue, K.; Liu, J.; Zhu, Y.; Xia, C.; Wang, P.; Zhang, J.; Kong, Y.; Wang, X.; Yan, Y.; Xia, B. Y. *In situ* ion-exchange preparation and topological transformation of trimetal-organic frameworks for efficient electrocatalytic water oxidation. *Energy Environ. Sci.* **2021**, *14*, 6546−6553.

(7) Zhou, J.; Li, R.; Fan, X.; Chen, Y.; Han, R.; Li, W.; Zheng, J.; Wang, B.; Li, X. Rational design of a metal-organic framework host for sulfur storage in fast, long-cycle Li-S batteries. *Energy Environ. Sci.* **2014**, *7*, 2715−2724.

(8) Thakur, A. K.; Majumder, M.; Patole, S. P.; Zaghib, K.; Reddy, M. V. Metal-organic framework-based materials: advances, exploits, and challenges in promoting post Li-ion battery technologies. *Mater. Adv.* **2021**, *2*, 2457−2482.

(9) Mehek, R.; Iqbal, N.; Noor, T.; Amjad, M. Z. B.; Ali, G.; Vignarooban, K.; Khan, M. A. Metal-organic framework based

electrode materials for lithium-ion batteries: a review. *RSC Adv.* **2021**, *11*, 29247−29266.
(10) Qian, Q.; Asinger, P. A.; Lee, M. J.; Han, G.; Mizrahi Rodriguez, K.; Lin, S.; Benedetti, F. M.; Wu, A. X.; Chi, W. S.; Smith, Z. P. MOF-based membranes for gas separations. *Chem. Rev.* **2020**, *120*, 8161−8266.
(11) Lin, R.-B.; Xiang, S.; Zhou, W.; Chen, B. Microporous metal-organic framework materials for gas separation. *Chem.* **2020**, *6*, 337−363.
(12) Koo, W.-T.; Jang, J.-S.; Qiao, S.; Hwang, W.; Jha, G.; Penner, R. M.; Kim, I.-D. Hierarchical metal-organic framework-assembled membrane filter for efficient removal of particulate matter. *ACS Appl. Mater. Interfaces* **2018**, *10*, 19957−19963.
(13) Yuan, H.; Li, N.; Fan, W.; Cai, H.; Zhao, D. Metal-Organic Framework Based Gas Sensors. *Adv. Sci.* **2022**, *9*, 2104374.
(14) Kreno, L. E.; Leong, K.; Farha, O. K.; Allendorf, M.; Van Duyne, R. P.; Hupp, J. T. Metal-organic framework materials as chemical sensors. *Chem. Rev.* **2012**, *112*, 1105−1125.
(15) Koo, W.-T.; Jang, J.-S.; Kim, I.-D. Metal-organic frameworks for chemiresistive sensors. *Chem.* **2019**, *5*, 1938−1963.
(16) Koo, W.-T.; Cho, H.-J.; Kim, D.-H.; Kim, Y. H.; Shin, H.; Penner, R. M.; Kim, I.-D. Chemiresistive hydrogen sensors: fundamentals, recent advances, and challenges. *ACS Nano* **2020**, *14*, 14284−14322.
(17) Jeong, S.-Y.; Kim, J.-S.; Lee, J.-H. Rational design of semiconductor-based chemiresistors and their libraries for next-generation artificial olfaction. *Adv. Mater.* **2020**, *32*, 2002075.
(18) Yang, H.; He, X.-W.; Wang, F.; Kang, Y.; Zhang, J. Doping copper into ZIF-67 for enhancing gas uptake capacity and visible-light-driven photocatalytic degradation of organic dye. *J. Mater. Chem.* **2012**, *22*, 21849−21851.
(19) Chen, E.-X.; Fu, H.-R.; Lin, R.; Tan, Y.-X.; Zhang, J. Highly selective and sensitive trimethylamine gas sensor based on cobalt imidazolate framework material. *ACS Appl. Mater. Interfaces* **2014**, *6*, 22871−22875.
(20) DMello, M. E.; Sundaram, N. G.; Singh, A.; Singh, A. K.; Kalidindi, S. B. An amine functionalized zirconium metal-organic framework as an effective chemiresistive sensor for acidic gases. *Chem. Commun.* **2019**, *55*, 349−352.
(21) Travlou, N. A.; Singh, K.; Rodriguez-Castellon, E.; Bandosz, T. J. Cu-BTC MOF-graphene-based hybrid materials as low concentration ammonia sensors. *J. Mater. Chem. A* **2015**, *3*, 11417−11429.
(22) Wang, M.; Dong, R.; Feng, X. Two-dimensional conjugated metal-organic frameworks (2D c-MOFs): chemistry and function for MOFtronics. *Chem. Soc. Rev.* **2021**, *50*, 2764−2793.
(23) Nam, K. W.; Park, S. S.; Dos Reis, R.; Dravid, V. P.; Kim, H.; Mirkin, C. A.; Stoddart, J. F. Conductive 2D metal-organic framework for high-performance cathodes in aqueous rechargeable zinc batteries. *Nat. Commun.* **2019**, *10*, 4948.
(24) Huang, X.; Sheng, P.; Tu, Z.; Zhang, F.; Wang, J.; Geng, H.; Zou, Y.; Di, C.-a.; Yi, Y.; Sun, Y.; Xu, W.; Zhu, D. A two-dimensional π-*d* conjugated coordination polymer with extremely high electrical conductivity and ambipolar transport behaviour. *Nat. Commun.* **2015**, *6*, 7408.
(25) Wu, G.; Huang, J.; Zang, Y.; He, J.; Xu, G. Porous field-effect transistors based on a semiconductive metal-organic framework. *J. Am. Chem. Soc.* **2017**, *139*, 1360−1363.
(26) Yoon, H.; Lee, S.; Oh, S.; Park, H.; Choi, S.; Oh, M. Synthesis of bimetallic conductive 2D metal-organic framework (Co_xNi_y-CAT) and its mass production: enhanced electrochemical oxygen reduction activity. *Small* **2019**, *15*, 1805232.
(27) Li, T.; Yin, W.; Gao, S.; Sun, Y.; Xu, P.; Wu, S.; Kong, H.; Yang, G.; Wei, G. The combination of two-dimensional nanomaterials with metal oxide nanoparticles for gas sensors: a review. *Nanomaterials* **2022**, *12*, 982.
(28) Kim, D.-H.; Kim, J. K.; Oh, D.; Park, S.; Kim, Y. B.; Ko, J.; Jung, W.; Kim, I.-D. Ex-Solution Hybrids Functionalized on Oxide Nanofibers for Highly Active and Durable Catalytic Materials. *ACS Nano* **2023**, *17*, 5842−5851.
(29) Song, L.; Ahn, J.; Xu, L.; Baek, J. W.; Shin, E.; Kim, I.-D. Facile Synthesis of Co_3O_4/$CoMoO_4$ Heterostructure Nanosheets for Enhanced Acetone Detection. *ACS Sens.* **2022**, *7*, 3540−3550.
(30) Kwon, B.; Bae, H.; Lee, H.; Kim, S.; Hwang, J.; Lim, H.; Lee, J. H.; Cho, K.; Ye, J.; Lee, S.; Lee, W. H. Ultrasensitive N-channel graphene gas sensors by nondestructive molecular doping. *ACS Nano* **2022**, *16*, 2176−2187.
(31) Choi, J. H.; Lee, J.; Byeon, M.; Hong, T. E.; Park, H.; Lee, C. Y. Graphene-based gas sensors with high sensitivity and minimal sensor-to-sensor variation. *ACS Appl. Nano Mater.* **2020**, *3*, 2257−2265.
(32) Shekhirev, M.; Lipatov, A.; Torres, A.; Vorobeva, N. S.; Harkleroad, A.; Lashkov, A.; Sysoev, V.; Sinitskii, A. Highly selective gas sensors based on graphene nanoribbons grown by chemical vapor deposition. *ACS Appl. Mater. Interfaces* **2020**, *12*, 7392−7402.
(33) Kang, J.-Y.; Koo, W.-T.; Jang, J.-S.; Kim, D.-H.; Jeong, Y. J.; Kim, R.; Ahn, J.; Choi, S.-J.; Kim, I.-D. 2D layer assembly of Pt-ZnO nanoparticles on reduced graphene oxide for flexible NO_2 sensors. *Sens. Actuators, B* **2021**, *331*, 129371.
(34) Burman, D.; Raha, H.; Manna, B.; Pramanik, P.; Guha, P. K. Substitutional doping of MoS_2 for superior gas-sensing applications: a proof of concept. *ACS Sens.* **2021**, *6*, 3398−3408.
(35) Pham, T.; Li, G.; Bekyarova, E.; Itkis, M. E.; Mulchandani, A. MoS_2-based optoelectronic gas sensor with sub-parts-per-billion limit of NO_2 gas detection. *ACS Nano* **2019**, *13*, 3196−3205.
(36) Koo, W. T.; Cha, J. H.; Jung, J. W.; Choi, S. J.; Jang, J. S.; Kim, D. H.; Kim, I. D. Few-layered WS_2 nanoplates confined in Co, N-doped hollow carbon nanocages: abundant WS_2 edges for highly sensitive gas sensors. *Adv. Funct. Mater.* **2018**, *28*, 1802575.
(37) Baek, J. W.; Kim, Y. H.; Ahn, J.; Kim, D.-H.; Shin, H.; Ko, J.; Park, S.; Park, C.; Shin, E.; Jang, J.-S.; Kim, I. D. Galvanic replacement reaction in perovskite oxide for superior chemiresistors. *J. Mater. Chem. A* **2022**, *10*, 23282−23293.
(38) Nascimento, E. P.; Firmino, H. C.; Neves, G. A.; Menezes, R. R. A review of recent developments in tin dioxide nanostructured materials for gas sensors. *Ceram. Int.* **2022**, *48*, 7405−7440.
(39) Zhou, T.; Zhang, T. Recent progress of nanostructured sensing materials from 0D to 3D: overview of structure-property-application relationship for gas sensors. *Small Methods* **2021**, *5*, 2100515.
(40) Burgués, J.; Marco, S. Low power operation of temperature-modulated metal oxide semiconductor gas sensors. *Sensors* **2018**, *18*, 339.
(41) Potyrailo, R. A.; Go, S.; Sexton, D.; Li, X.; Alkadi, N.; Kolmakov, A.; Amm, B.; St-Pierre, R.; Scherer, B.; Nayeri, M.; et al. Extraordinary performance of semiconducting metal oxide gas sensors using dielectric excitation. *Nat. Electron.* **2020**, *3*, 280−289.
(42) Rasch, F.; Postica, V.; Schütt, F.; Mishra, Y. K.; Nia, A. S.; Lohe, M. R.; Feng, X.; Adelung, R.; Lupan, O. Highly selective and ultra-low power consumption metal oxide based hydrogen gas sensor employing graphene oxide as molecular sieve. *Sens. Actuators, B* **2020**, *320*, 128363.
(43) Luo, Y.; Abidian, M. R.; Ahn, J.-H.; Akinwande, D.; Andrews, A. M.; Antonietti, M.; Bao, Z.; Berggren, M.; Berkey, C. A.; Bettinger, C. J.; et al. Technology roadmap for flexible sensors. *ACS Nano* **2023**, *17*, 5211−5295.
(44) Yang, L.; Yi, N.; Zhu, J.; Cheng, Z.; Yin, X.; Zhang, X.; Zhu, H.; Cheng, H. Novel gas sensing platform based on a stretchable laser-induced graphene pattern with self-heating capabilities. *J. Mater. Chem. A* **2020**, *8*, 6487−6500.
(45) Kim, D.-H.; Cha, J.-H.; Shim, G.; Kim, Y. H.; Jang, J.-S.; Shin, H.; Ahn, J.; Choi, S.-Y.; Kim, I.-D. Flash-thermochemical engineering of phase and surface activity on metal oxides. *Chem.* **2022**, *8*, 1014−1033.
(46) Yu, T.; Cheng, X.; Zhang, X.; Sui, L.; Xu, Y.; Gao, S.; Zhao, H.; Huo, L. Highly sensitive H_2S detection sensors at low temperature based on hierarchically structured NiO porous nanowall arrays. *J. Mater. Chem. A* **2015**, *3*, 11991−11999.
(47) Shin, E.; Kim, D.-H.; Cha, J.-H.; Yun, S.; Shin, H.; Ahn, J.; Jang, J.-S.; Baek, J. W.; Park, C.; Ko, J.; et al. Ultrafast Ambient-Air

Exsolution on Metal Oxide via Momentary Photothermal Effect. *ACS Nano* **2022**, *16*, 18133−18142.
(48) Xiangfeng, C.; Siciliano, P. CH3SH-sensing characteristics of $LaFeO_3$ thick-film prepared by co-precipitation method. *Sens. Actuators, B* **2003**, *94*, 197−200.
(49) Shin, H.; Kim, D.-H.; Jung, W.; Jang, J.-S.; Kim, Y. H.; Lee, Y.; Chang, K.; Lee, J.; Park, J.; Namkoong, K.; et al. Surface activity-tuned metal oxide chemiresistor: toward direct and quantitative halitosis diagnosis. *ACS Nano* **2021**, *15*, 14207−14217.
(50) Huang, X.; Gong, Z.; Lv, Y. Advances in metal-organic frameworks-based gas sensors for hazardous substances. *TrAC, Trends Anal. Chem.* **2022**, *153*, 116644.
(51) Jo, Y. M.; Jo, Y. K.; Lee, J. H.; Jang, H. W.; Hwang, I. S.; Yoo, D. J. MOF-Based Chemiresistive Gas Sensors: Toward New Functionalities. *Adv. Mater.* **2023**, 2206842.
(52) Yao, M.-S.; Li, W.-H.; Xu, G. Metal-organic frameworks and their derivatives for electrically-transduced gas sensors. *Coord. Chem. Rev.* **2021**, *426*, 213479.
(53) Zhang, L. T.; Zhou, Y.; Han, S. T. The role of metal-organic frameworks in electronic sensors. *Angew. Chem.* **2021**, *133*, 15320−15340.
(54) Li, H.-Y.; Zhao, S.-N.; Zang, S.-Q.; Li, J. Functional metal-organic frameworks as effective sensors of gases and volatile compounds. *Chem. Soc. Rev.* **2020**, *49*, 6364−6401.
(55) Campbell, M. G.; Dincă, M. Metal-organic frameworks as active materials in electronic sensor devices. *Sensors* **2017**, *17*, 1108.
(56) Liu, J.; Chen, Y.; Feng, X.; Dong, R. Conductive 2D Conjugated Metal-Organic Framework Thin Films: Synthesis and Functions for (Opto-) electronics. *Small Struct.* **2022**, *3*, 2100210.
(57) Ko, M.; Mendecki, L.; Mirica, K. A. Conductive two-dimensional metal-organic frameworks as multifunctional materials. *Chem. Commun.* **2018**, *54*, 7873−7891.
(58) Xie, L. S.; Skorupskii, G.; Dincă, M. Electrically conductive metal-organic frameworks. *Chem. Rev.* **2020**, *120*, 8536−8580.
(59) Zhang, R.; Lu, L.; Chang, Y.; Liu, M. Gas sensing based on metal-organic frameworks: Concepts, functions, and developments. *J. Hazard. Mater.* **2022**, *429*, 128321.
(60) Meng, Z.; Aykanat, A.; Mirica, K. A. Welding metallophthalocyanines into bimetallic molecular meshes for ultrasensitive, low-power chemiresistive detection of gases. *J. Am. Chem. Soc.* **2019**, *141*, 2046−2053.
(61) Yao, M.-S.; Wang, P.; Gu, Y.-F.; Koganezawa, T.; Ashitani, H.; Kubota, Y.; Wang, Z.-M.; Fan, Z.-Y.; Otake, K.-i.; Kitagawa, S. A comparative study of honeycomb-like 2D π-conjugated metal-organic framework chemiresistors: conductivity and channels. *Dalton Transactions* **2021**, *50*, 13236−13245.
(62) Wu, A.-Q.; Wang, W.-Q.; Zhan, H.-B.; Cao, L.-A.; Ye, X.-L.; Zheng, J.-J.; Kumar, P. N.; Chiranjeevulu, K.; Deng, W.-H.; Wang, G.-E.; et al. Layer-by-layer assembled dual-ligand conductive MOF nanofilms with modulated chemiresistive sensitivity and selectivity. *Nano Res.* **2021**, *14*, 438−443.
(63) Jiang, Q.; Xiong, P.; Liu, J.; Xie, Z.; Wang, Q.; Yang, X. Q.; Hu, E.; Cao, Y.; Sun, J.; Xu, Y.; et al. A redox-active 2D metal-organic framework for efficient lithium storage with extraordinary high capacity. *Angew. Chem., Int. Ed.* **2020**, *59*, 5273−5277.
(64) Miner, E. M.; Wang, L.; Dincă, M. Modular O_2 electroreduction activity in triphenylene-based metal-organic frameworks. *Chemical Science* **2018**, *9*, 6286−6291.
(65) Zhong, H.; Ly, K. H.; Wang, M.; Krupskaya, Y.; Han, X.; Zhang, J.; Zhang, J.; Kataev, V.; Büchner, B.; Weidinger, I. M.; et al. A phthalocyanine-based layered two-dimensional conjugated metal-organic framework as a highly efficient electrocatalyst for the oxygen reduction reaction. *Angew. Chem., Int. Ed.* **2019**, *58*, 10677−10682.
(66) Feng, D.; Lei, T.; Lukatskaya, M. R.; Park, J.; Huang, Z.; Lee, M.; Shaw, L.; Chen, S.; Yakovenko, A. A.; Kulkarni, A.; et al. Robust and conductive two-dimensional metal-organic frameworks with exceptionally high volumetric and areal capacitance. *Nat. Energy* **2018**, *3*, 30−36.
(67) Park, J.; Lee, M.; Feng, D.; Huang, Z.; Hinckley, A. C.; Yakovenko, A.; Zou, X.; Cui, Y.; Bao, Z. Stabilization of hexaaminobenzene in a 2D conductive metal-organic framework for high power sodium storage. *J. Am. Chem. Soc.* **2018**, *140*, 10315−10323.
(68) Sheberla, D.; Sun, L.; Blood-Forsythe, M. A.; Er, S. l.; Wade, C. R.; Brozek, C. K.; Aspuru-Guzik, A.; Dincă, M. High electrical conductivity in Ni_3(2, 3, 6, 7, 10, 11-hexaiminotriphenylene)$_2$, a semiconducting metal-organic graphene analogue. *J. Am. Chem. Soc.* **2014**, *136*, 8859−8862.
(69) Jia, H.; Yao, Y.; Zhao, J.; Gao, Y.; Luo, Z.; Du, P. A novel two-dimensional nickel phthalocyanine-based metal-organic framework for highly efficient water oxidation catalysis. *J. Mater. Chem. A* **2018**, *6*, 1188−1195.
(70) Lian, Y.; Yang, W.; Zhang, C.; Sun, H.; Deng, Z.; Xu, W.; Song, L.; Ouyang, Z.; Wang, Z.; Guo, J.; et al. Unpaired 3d electrons on atomically dispersed cobalt centres in coordination polymers regulate both oxygen reduction reaction (ORR) activity and selectivity for use in zinc-air batteries. *Angew. Chem., Int. Ed.* **2020**, *59*, 286−294.
(71) Wang, M.; Shi, H.; Zhang, P.; Liao, Z.; Wang, M.; Zhong, H.; Schwotzer, F.; Nia, A. S.; Zschech, E.; Zhou, S.; et al. Phthalocyanine-based 2D conjugated metal-organic framework nanosheets for high-performance micro-supercapacitors. *Adv. Funct. Mater.* **2020**, *30*, 2002664.
(72) Cui, J.; Xu, Z. An electroactive porous network from covalent metal-dithiolene links. *Chem. Commun.* **2014**, *50*, 3986−3988.
(73) Dong, R.; Han, P.; Arora, H.; Ballabio, M.; Karakus, M.; Zhang, Z.; Shekhar, C.; Adler, P.; Petkov, P. S.; Erbe, A.; et al. High-mobility band-like charge transport in a semiconducting two-dimensional metal-organic framework. *Nat. Mater.* **2018**, *17*, 1027−1032.
(74) Hmadeh, M.; Lu, Z.; Liu, Z.; Gándara, F.; Furukawa, H.; Wan, S.; Augustyn, V.; Chang, R.; Liao, L.; Zhou, F.; et al. New porous crystals of extended metal-catecholates. *Chem. Mater.* **2012**, *24*, 3511−3513.
(75) Park, J.; Hinckley, A. C.; Huang, Z.; Feng, D.; Yakovenko, A. A.; Lee, M.; Chen, S.; Zou, X.; Bao, Z. Synthetic routes for a 2D semiconductive copper hexahydroxybenzene metal-organic framework. *J. Am. Chem. Soc.* **2018**, *140*, 14533−14537.
(76) Nagatomi, H.; Yanai, N.; Yamada, T.; Shiraishi, K.; Kimizuka, N. Synthesis and electric properties of a two-dimensional metal-organic framework based on phthalocyanine. *Chem.—Eur. J.* **2018**, *24*, 1806−1810.
(77) Clough, A. J.; Skelton, J. M.; Downes, C. A.; De La Rosa, A. A.; Yoo, J. W.; Walsh, A.; Melot, B. C.; Marinescu, S. C. Metallic conductivity in a two-dimensional cobalt dithiolene metal-organic framework. *J. Am. Chem. Soc.* **2017**, *139*, 10863−10867.
(78) Clough, A. J.; Orchanian, N. M.; Skelton, J. M.; Neer, A. J.; Howard, S. A.; Downes, C. A.; Piper, L. F.; Walsh, A.; Melot, B. C.; Marinescu, S. C. Room temperature metallic conductivity in a metal-organic framework induced by oxidation. *J. Am. Chem. Soc.* **2019**, *141*, 16323−16330.
(79) Mähringer, A.; Jakowetz, A. C.; Rotter, J. M.; Bohn, B. J.; Stolarczyk, J. K.; Feldmann, J.; Bein, T.; Medina, D. D. Oriented thin films of electroactive triphenylene catecholate-based two-dimensional metal-organic frameworks. *ACS Nano* **2019**, *13*, 6711−6719.
(80) Wu, H.; Zhang, W.; Kandambeth, S.; Shekhah, O.; Eddaoudi, M.; Alshareef, H. N. Conductive metal-organic frameworks selectively grown on laser-scribed graphene for electrochemical microsupercapacitors. *Adv. Energy Mater.* **2019**, *9*, 1900482.
(81) Song, X.; Wang, X.; Li, Y.; Zheng, C.; Zhang, B.; Di, C. a.; Li, F.; Jin, C.; Mi, W.; Chen, L.; et al. 2D semiconducting metal-organic framework thin films for organic spin valves. *Angew. Chem., Int. Ed.* **2020**, *59*, 1118−1123.
(82) Huang, X.; Zhang, S.; Liu, L.; Yu, L.; Chen, G.; Xu, W.; Zhu, D. Superconductivity in a copper (II)-based coordination polymer with perfect Kagome structure. *Angew. Chem.* **2018**, *130*, 152−156.
(83) Huang, X.; Yao, H.; Cui, Y.; Hao, W.; Zhu, J.; Xu, W.; Zhu, D. Conductive copper benzenehexathiol coordination polymer as a

hydrogen evolution catalyst. *ACS Appl. Mater. Interfaces* **2017**, *9*, 40752−40759.
(84) Pal, T.; Kambe, T.; Kusamoto, T.; Foo, M. L.; Matsuoka, R.; Sakamoto, R.; Nishihara, H. Interfacial synthesis of electrically conducting palladium bis(dithiolene) complex nanosheet. *ChemPlusChem.* **2015**, *80*, 1255−1258.
(85) Dou, J.-H.; Sun, L.; Ge, Y.; Li, W.; Hendon, C. H.; Li, J.; Gul, S.; Yano, J.; Stach, E. A.; Dincă, M. Signature of metallic behavior in the metal-organic frameworks M_3(hexaiminobenzene)$_2$ (M = Ni, Cu). *J. Am. Chem. Soc.* **2017**, *139*, 13608−13611.
(86) Ko, M.; Aykanat, A.; Smith, M. K.; Mirica, K. A. Drawing sensors with ball-milled blends of metal-organic frameworks and graphite. *Sensors* **2017**, *17*, 2192.
(87) Day, R. W.; Bediako, D. K.; Rezaee, M.; Parent, L. R.; Skorupskii, G.; Arguilla, M. Q.; Hendon, C. H.; Stassen, I.; Gianneschi, N. C.; Kim, P.; Dincă, M. Single crystals of electrically conductive two-dimensional metal-organic frameworks: Structural and electrical transport properties. *ACS Cent. Sci.* **2019**, *5*, 1959−1964.
(88) Chen, T.; Dou, J.-H.; Yang, L.; Sun, C.; Libretto, N. J.; Skorupskii, G.; Miller, J. T.; Dincă, M. Continuous electrical conductivity variation in M_3(hexaiminotriphenylene)$_2$ (M = Co, Ni, Cu) MOF alloys. *J. Am. Chem. Soc.* **2020**, *142*, 12367−12373.
(89) Kambe, T.; Sakamoto, R.; Hoshiko, K.; Takada, K.; Miyachi, M.; Ryu, J.-H.; Sasaki, S.; Kim, J.; Nakazato, K.; Takata, M.; Nishihara, H. π-Conjugated nickel bis(dithiolene) complex nanosheet. *J. Am. Chem. Soc.* **2013**, *135*, 2462−2465.
(90) Kambe, T.; Sakamoto, R.; Kusamoto, T.; Pal, T.; Fukui, N.; Hoshiko, K.; Shimojima, T.; Wang, Z.; Hirahara, T.; Ishizaka, K.; Nishihara, H.; et al. Redox control and high conductivity of nickel bis(dithiolene) complex π-nanosheet: a potential organic two-dimensional topological insulator. *J. Am. Chem. Soc.* **2014**, *136*, 14357−14360.
(91) Skorupskii, G.; Trump, B. A.; Kasel, T. W.; Brown, C. M.; Hendon, C. H.; Dincă, M. Efficient and tunable one-dimensional charge transport in layered lanthanide metal-organic frameworks. *Nat. Chem.* **2020**, *12*, 131−136.
(92) Lukose, B.; Kuc, A.; Heine, T. The structure of layered covalent-organic frameworks. *Chem.—Eur. J.* **2011**, *17*, 2388−2392.
(93) Dou, J.-H.; Arguilla, M. Q.; Luo, Y.; Li, J.; Zhang, W.; Sun, L.; Mancuso, J. L.; Yang, L.; Chen, T.; Parent, L. R.; et al. Atomically precise single-crystal structures of electrically conducting 2D metal-organic frameworks. *Nat. Mater.* **2021**, *20*, 222−228.
(94) Rubio-Giménez, V.; Almora-Barrios, N.; Escorcia-Ariza, G.; Galbiati, M.; Sessolo, M.; Tatay, S.; Martí-Gastaldo, C. Origin of the chemiresistive response of ultrathin films of conductive metal-organic frameworks. *Angew. Chem.* **2018**, *130*, 15306−15310.
(95) Stolz, R. M.; Mahdavi-Shakib, A.; Frederick, B. G.; Mirica, K. A. Host-Guest Interactions and Redox Activity in Layered Conductive Metal-Organic Frameworks. *Chem. Mater.* **2020**, *32*, 7639−7652.
(96) Meng, Z.; Stolz, R. M.; Mirica, K. A. Two-dimensional chemiresistive covalent organic framework with high intrinsic conductivity. *J. Am. Chem. Soc.* **2019**, *141*, 11929−11937.
(97) Campbell, M. G.; Liu, S. F.; Swager, T. M.; Dinca, M. Chemiresistive sensor arrays from conductive 2D metal-organic frameworks. *J. Am. Chem. Soc.* **2015**, *137*, 13780−13783.
(98) Yao, M. S.; Lv, X. J.; Fu, Z. H.; Li, W. H.; Deng, W. H.; Wu, G. D.; Xu, G. Layer-by-layer assembled conductive metal-organic framework nanofilms for room-temperature chemiresistive sensing. *Angew. Chem., Int. Ed.* **2017**, *56*, 16510−16514.
(99) Jo, Y.-M.; Lim, K.; Yoon, J. W.; Jo, Y. K.; Moon, Y. K.; Jang, H. W.; Lee, J.-H. Visible-light-activated Type II heterojunction in Cu_3(hexahydroxytriphenylene)$_2$/Fe_2O_3 hybrids for reversible NO_2 sensing: Critical role of π-π* transition. *ACS Central Science* **2021**, *7*, 1176−1182.
(100) Gao, J.; Geng, S.; Chen, Y.; Cheng, P.; Zhang, Z. Theoretical exploration and electronic applications of conductive two-dimensional metal-organic frameworks. *Top. Curr. Chem.* **2020**, *378*, 25.
(101) Smith, M. K.; Jensen, K. E.; Pivak, P. A.; Mirica, K. A. Direct self-assembly of conductive nanorods of metal-organic frameworks into chemiresistive devices on shrinkable polymer films. *Chem. Mater.* **2016**, *28*, 5264−5268.
(102) Smith, M. K.; Mirica, K. A. Self-organized frameworks on textiles (SOFT): conductive fabrics for simultaneous sensing, capture, and filtration of gases. *J. Am. Chem. Soc.* **2017**, *139*, 16759−16767.
(103) Dong, R.; Pfeffermann, M.; Liang, H.; Zheng, Z.; Zhu, X.; Zhang, J.; Feng, X. Large-area, free-standing, two-dimensional supramolecular polymer single-layer sheets for highly efficient electrocatalytic hydrogen evolution. *Angew. Chem., Int. Ed.* **2015**, *54*, 12058−12063.
(104) Kim, J.-O.; Koo, W.-T.; Kim, H.; Park, C.; Lee, T.; Hutomo, C. A.; Choi, S. Q.; Kim, D. S.; Kim, I.-D.; Park, S. Large-area synthesis of nanoscopic catalyst-decorated conductive MOF film using microfluidic-based solution shearing. *Nat. Commun.* **2021**, *12*, 4294.
(105) Campbell, M. G.; Sheberla, D.; Liu, S. F.; Swager, T. M.; Dincă, M. Cu_3(hexaiminotriphenylene)$_2$: an electrically conductive 2D metal-organic framework for chemiresistive sensing. *Angew. Chem., Int. Ed.* **2015**, *54*, 4349−4352.
(106) Yao, M. S.; Zheng, J. J.; Wu, A. Q.; Xu, G.; Nagarkar, S. S.; Zhang, G.; Tsujimoto, M.; Sakaki, S.; Horike, S.; Otake, K.; et al. A Dual-Ligand Porous Coordination Polymer Chemiresistor with Modulated Conductivity and Porosity. *Angew. Chem., Int. Ed.* **2020**, *59*, 172−176.
(107) Stassen, I.; Dou, J.-H.; Hendon, C.; Dincă, M. Chemiresistive sensing of ambient CO_2 by an autogenously hydrated Cu_3(hexaiminobenzene)$_2$ framework. *ACS Cent. Sci.* **2019**, *5*, 1425−1431.
(108) Aykanat, A.; Meng, Z.; Stolz, R. M.; Morrell, C. T.; Mirica, K. A. Bimetallic Two-Dimensional Metal-Organic Frameworks for the Chemiresistive Detection of Carbon Monoxide. *Angew. Chem., Int. Ed.* **2022**, *61*, No. e202113665.
(109) Su, X.; Zhong, Z.; Yan, X.; Zhang, T.; Wang, C.; Wang, Y.-X.; Xu, G.; Chen, L. Facile Synthesis of Metallosalphen-Based 2D Conductive Metal-Organic Frameworks for NO_2 Sensing: Metal Coordination Induced Planarization. *Angew. Chem., Int. Ed.* **2023**, *62*, No. e202302645.
(110) Hoppe, B.; Hindricks, K. D.; Warwas, D. P.; Schulze, H. A.; Mohmeyer, A.; Pinkvos, T. J.; Zailskas, S.; Krey, M. R.; Belke, C.; König, S.; et al. Graphene-like metal-organic frameworks: morphology control, optimization of thin film electrical conductivity and fast sensing applications. *CrystEngComm* **2018**, *20*, 6458−6471.
(111) Liu, C.; Gu, Y.; Liu, C.; Liu, S.; Li, X.; Ma, J.; Ding, M. Missing-linker 2D conductive metal organic frameworks for rapid gas detection. *ACS sens.* **2021**, *6*, 429−438.
(112) Chen, X.; Lu, Y.; Dong, J.; Ma, L.; Yi, Z.; Wang, Y.; Wang, L.; Wang, S.; Zhao, Y.; Huang, J.; et al. Ultrafast In Situ Synthesis of Large-Area Conductive Metal-Organic Frameworks on Substrates for Flexible Chemiresistive Sensing. *ACS Appl. Mater. Interfaces* **2020**, *12*, 57235−57244.
(113) Zheng, R.; Fu, Z. H.; Deng, W. H.; Wen, Y.; Wu, A. Q.; Ye, X. L.; Xu, G. The Growth Mechanism of a Conductive MOF Thin Film in Spray-based Layer-by-layer Liquid Phase Epitaxy. *Angew. Chem., Int. Ed.* **2022**, *61*, No. e202212797.
(114) Lin, Y.; Li, W. H.; Wen, Y.; Wang, G. E.; Ye, X. L.; Xu, G. Layer-by-Layer growth of preferred-oriented MOF thin film on nanowire array for high-performance chemiresistive sensing. *Angew. Chem., Int. Ed.* **2021**, *60*, 25758−25761.
(115) Lee, T.; Kim, J. O.; Park, C.; Kim, H.; Kim, M.; Park, H.; Kim, I.; Ko, J.; Pak, K.; Choi, S. Q.; et al. Large-Area Synthesis of Ultrathin, Flexible, and Transparent Conductive Metal-Organic Framework Thin Films via a Microfluidic-Based Solution Shearing Process. *Adv. Mater.* **2022**, *34*, 2107696.
(116) Park, S.; Oh, D.; Ahn, J.; Kim, J. K.; Kim, D. H.; Kim, S.; Park, C.; Jung, W.; Kim, I. D. Promoting Ex-Solution from Metal-Organic-Framework-Mediated Oxide Scaffolds for Highly Active and Robust Catalysts. *Adv. Mater.* **2022**, *34*, 2201109.

https://doi.org/10.1021/acsnanoscienceau.3c00024
ACS Nanosci. Au 2023, 3, 353−374

(117) Zhang, W.; Lu, G.; Cui, C.; Liu, Y.; Li, S.; Yan, W.; Xing, C.; Chi, Y. R.; Yang, Y.; Huo, F. A family of metal-organic frameworks exhibiting size-selective catalysis with encapsulated noble-metal nanoparticles. *Adv. Mater.* **2014**, *26*, 4056−4060.
(118) Koo, W.-T.; Choi, S.-J.; Kim, S.-J.; Jang, J.-S.; Tuller, H. L.; Kim, I.-D. Heterogeneous sensitization of metal-organic framework driven metal@metal oxide complex catalysts on an oxide nanofiber scaffold toward superior gas sensors. *J. Am. Chem. Soc.* **2016**, *138*, 13431−13437.
(119) Jang, J.-S.; Koo, W.-T.; Choi, S.-J.; Kim, I.-D. Metal organic framework-templated chemiresistor: sensing type transition from P-to-N using hollow metal oxide polyhedron via galvanic replacement. *J. Am. Chem. Soc.* **2017**, *139*, 11868−11876.
(120) Koo, W. T.; Kim, S. J.; Jang, J. S.; Kim, D. H.; Kim, I. D. Catalytic metal nanoparticles embedded in conductive metal-organic frameworks for chemiresistors: highly active and conductive porous materials. *Adv. Sci.* **2019**, *6*, 1900250.
(121) Sun, Y.; Wang, B.; Hou, Y.; Suematsu, K.; Zhao, Z.; Zhang, W.; Shimanoe, K.; Hu, J. Noble metal nanoparticles functionalized conductive Co_3(hexaiminotriphenylene)$_2$ chemiresistor for hydrogen sulfide detection at Room-Temperature. *Chem. Eng. J.* **2023**, *465*, 142818.
(122) Park, C.; Koo, W. T.; Chong, S.; Shin, H.; Kim, Y. H.; Cho, H. J.; Jang, J. S.; Kim, D. H.; Lee, J.; Park, S.; et al. Confinement of Ultrasmall Bimetallic Nanoparticles in Conductive Metal-Organic Frameworks via Site-Specific Nucleation. *Adv. Mater.* **2021**, *33*, 2101216.
(123) Choi, H. J.; Chung, J.-H.; Yoon, J.-W.; Lee, J.-H. Highly selective, sensitive, and rapidly responding acetone sensor using ferroelectric ϵ-WO_3 spheres doped with Nb for monitoring ketogenic diet efficiency. *Sens. Actuators, B* **2021**, *338*, 129823.
(124) Wang, M.; Zhang, Z.; Zhong, H.; Huang, X.; Li, W.; Hambsch, M.; Zhang, P.; Wang, Z.; St. Petkov, P.; Heine, T.; et al. Surface-Modified Phthalocyanine-Based Two-Dimensional Conjugated Metal-Organic Framework Films for Polarity-Selective Chemiresistive Sensing. *Angew. Chem.* **2021**, *133*, 18814−18820.
(125) Kim, D. H.; Chong, S.; Park, C.; Ahn, J.; Jang, J. S.; Kim, J.; Kim, I. D. Oxide/ZIF-8 Hybrid Nanofiber Yarns: Heightened Surface Activity for Exceptional Chemiresistive Sensing. *Adv. Mater.* **2022**, *34*, 2105869.
(126) Yao, M. S.; Xiu, J. W.; Huang, Q. Q.; Li, W. H.; Wu, W. W.; Wu, A. Q.; Cao, L. A.; Deng, W. H.; Wang, G. E.; Xu, G. Van der Waals Heterostructured MOF-on-MOF Thin Films: Cascading Functionality to Realize Advanced Chemiresistive Sensing. *Angew. Chem.* **2019**, *131*, 15057−15061.
(127) Cho, S. R.; Kim, D. H.; Jeon, M.; Rani, P.; Gyeon, M.; Kim, Y.; Jo, M. k.; Song, S.; Park, J. Y.; Kim, J.; et al. Overlaying Monolayer Metal-Organic Framework on $PtSe_2$-Based Gas Sensor for Tuning Selectivity. *Adv. Funct. Mater.* **2022**, *32*, 2207265.
(128) Kwon, O.; Kim, J. Y.; Park, S.; Lee, J. H.; Ha, J.; Park, H.; Moon, H. R.; Kim, J. Computer-aided discovery of connected metal-organic frameworks. *Nat. Commun.* **2019**, *10*, 3620.
(129) Cho, S.; Park, C.; Jeon, M.; Lee, J. H.; Kwon, O.; Seong, S.; Kim, J.; Kim, I.-D.; Moon, H. R. Interface-sensitized chemiresistor: Integrated conductive and porous metal-organic frameworks. *Chem. Eng. J.* **2022**, *449*, 137780.

https://doi.org/10.1021/acsnanoscienceau.3c00024
ACS Nanosci. Au 2023, 3, 353−374